A review on recent developments of thermoelectric materials for room-temperature applications

Zohreh Soleimani[a,*], Stamatis Zoras[a], Boris Ceranic[a], Sally Shahzad[b], Yuanlong Cui[a]

[a] Department of Built Environment, College of Engineering and Technology, University of Derby, DE22 3AW, Derby, UK
[b] Sheffield School of Architecture, University of Sheffield, S10 2TN, Sheffield, UK

Abstract

Wearable thermoelectric generators (TEGs) emerge as a viable renewable energy source, which directly convert the heat dissipated from human skin into electricity. Extensive reviews have been conducted on the efficiency of thermoelectric materials (TE) as the dominant element of TEGs. TE materials are categorised as inorganic, organic, and hybrid. Each of these reviews focused on either a specific type of TE materials, or on a certain specification (i.e. flexibility) of them. However, less attention has been paid to comprehensively review all these types without taking into account a certain specification. Therefore, the purpose of this paper is to summarize the progress and current state-of-the-art research on the three types of TE materials respecting their TE properties and efficiency at 300K, which is the operating temperature of wearable TEGs. Concerning the inorganic TE materials, the results show that $Bi_{0.4-x}Sb_{1.6+x}Te_3$ and $Bi_2Te_{2.7}Se_{0.3}$ are the most optimal TE materials, which exhibit the greatest efficiencies at room temperature. In addition, it is remarkably more efficient to replace polymer based TE composites with carbon based TE composites in the organic and the hybrid types. In total, this comprehensive review paves the way for researchers to find out the most suitable TE materials at room temperatures.

Keywords: Thermoelectric materials, energy harvesting, wearable, power generation

Contents

Nomenclature

Symbols		Abbreviations	
α	Seebeck coefficient (μV/K)	TE	thermoelectric module
σ	electrical conductivity (S/cm)	TEG	thermoelectric generator
λ	thermal conductivity (W/mK)	PF	power factor
$Z\overline{T}$	figure of merit	GHG	greenhouse gas
T_H	temperature of hot reservoirs		
T_C	temperature of cold reservoirs		

1.   Introduction

Owing to the global climate warming and shortage of fossil fuel reserves, using renewable energy sources are gaining more attention than any time before. In 2016, fossil fuels generated 67.3% of total world gross electricity production [1] , which was equivalent to 16319.58 TWh [2]. Meanwhile, more than 60% of the primary energy of fossil fuels is being lost as waste heat [3]. To overcome the associated greenhouse gas (GHG) emission and environmental degradation, the share of renewables (i.e., hydro, wind, solar PV, geothermal and tide) in the electricity sector is expected to grow from 23.8% in 2016 to 29.4% in 2023 [4]. Among the various power technologies, thermoelectric generators (TEGs) are striking candidates for solving the energy problem from an environmental-sustainable viewpoint. Because they convert the temperature difference between the hot end and surrounding ambient directly into

the electrical energy by carrier motion in the solid. Therefore, they have the advantages of harvesting the thermal energy generated from natural heat sources (such as solar, geothermal and human body) and ubiquitous waste heat (such as motor vehicles and industrial sector) [5].

Over the last decades, there is a fundamental breakthrough in the field of portable electronics such as wearable electronics, smart clothes and implantable medical devices [6]. In the meantime, battery is the preeminent power supply source of portable electronics due to its readiness and high power bandwidth, but subject to periodic recharging and replacement. Some wearable electronics, such as medical sensors for elderly people, require an extended service time without user's intervention. These deficiencies in batteries have led to focused research efforts on replacing the batteries with wearable TEGs, which utilize the temperature difference between body skin and ambient to generate a low level of power current (from several μV to mV). In particular, wearable TEGs implement Seebeck effect, which was founded in 1821 by German scientist Thomas J. Seebec. According to Seebeck effect, a circuit consisted of two dissimilar conductors (or semiconductors) has the high potential of yielding an electromotive force when one junction is heated [7]. The conventional configuration of a wearable TEG is simplified in Fig. 1.
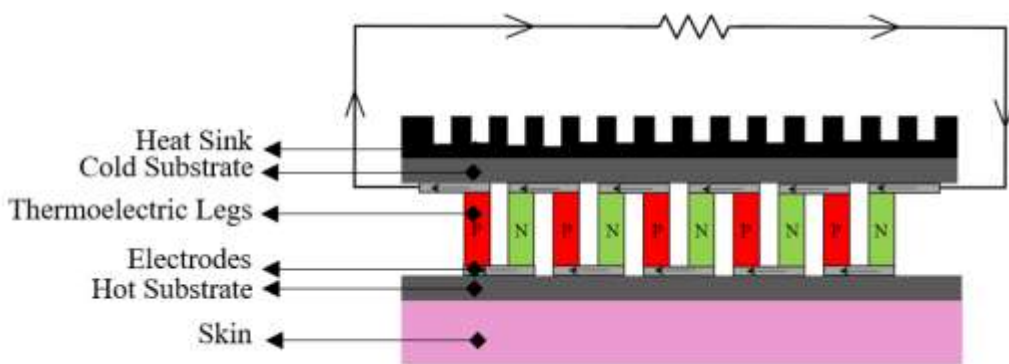
Fig. 1. Schematic diagram showing components and arrangement of a typical wearable TE module.

Even though, the average heat generated by human body is in the range between 100 to 525W [8], but the thermal resistance of the body precludes a considerable fraction of this heat from dissipation. Therefore, the low effective temperature difference between human skin and ambient is an inevitable barrier in efficiency of wearable TEGs. For current commercial wearable TEGs, the power generation efficiency, which is quantified by a figure of merit $(Z\overline{T})$, is lower than 1. Obviously, such a low efficiency value is not competitive against conventional power generations, as shown in Fig. 2. However, wearable TEGs still find niche

3

application because of their solid-state operation, easy fabrication, vast scalability, noiseless operation, maintenance- free operation, no chemical reactions, and exceptional reliability [9-11].
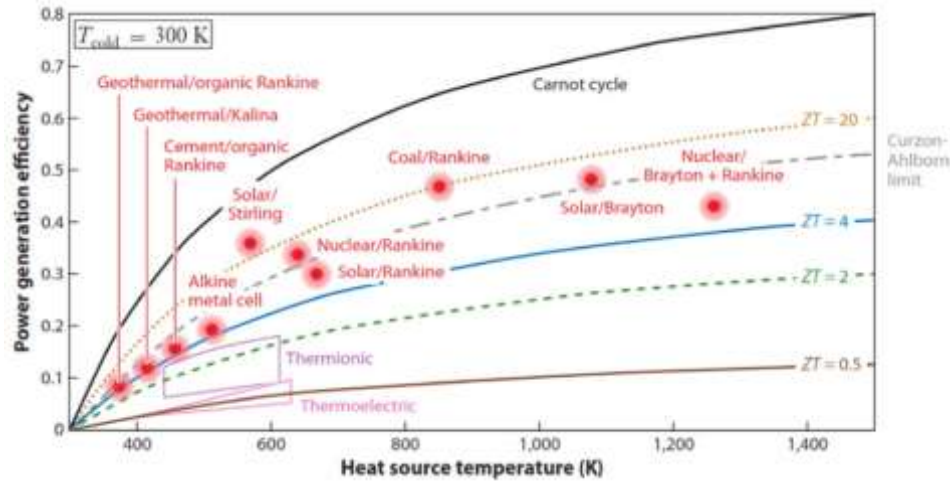
Fig. 2. Comparison of power generation systems [12].

To fit in the large-scale portable electronics, there have been great efforts in rational design of wearable TEGs and energy conversion efficicency of TE materials. The conversion efficicency depends on two crusial factors: (1) the operating temperature, (2) and properties of the TE materials. Regarding wearable TEGs, the operating temperature, which is the temperature difference between the human body (normally 310K) and the ambient temperature (300K), is almost constant. However, the properties of TE materials can be improved by various strategies, including point defect engineering, band engineering, structural nano crystallization, interface engineering, and hierarchical architecting [13].

In general, there are three types of TE materials: inorganic, organic and inorganic/organic hybrids. Table 1 summarizes the typical TE materials applicable for wearable TEGs regarding their categories. The first type refers to the materials consisted of inorganic composites, for example, bismuth telluride (BiTe), tin selenide (SnSe), lead telluride (PbTe), and silicon-germanium (SiGe). The second type refers to TE materials, which their active material is dominantly a conducting polymer such as poly (3,4-ethylenedioxythiophene): poly (styrenesulfonate) (PEDOT:PSS), polyaniline(PANI), and polypyrrole (PPY) . Finally, hybrid TE materials composed of an inorganic material (such as metal-based chemicals) as an additive doped into an organic material as a matrix. To illustrate, BiTe – PEDOT:PSS is a hybrid TE material consist of an inorganic metal compound and a conducting polymer. Although, there

4

are some TE materials available in labs with $Z\overline{T}$ value of 2, but the target $Z\overline{T}$ value is 3 or greater [14].

Table 1. Summary of the main categories of TE materials usable in wearable TEGs.

TE Materials

Inorganic	Organic	Hybrid (Inorganic/Organic)
Bi_2Te_3	PEDOT:PSS	Te-PEDOT:PSS
$Bi_{0.5}Sb_{1.5}Te_3$	PEDOT:S-PHE	SWCNT/PC-Te
$Bi_2Te_{2.7}Se_{0.3}$	PBTTT	Te NWs/PEDOT NWs
$Bi_{0.4}Sb_{1.59}Ge_{0.01}Te_3$	PDTDE	Te- MWCNT/PANI
$Sb_{1.85}In_{0.15}Te_3$	PBDT-TT-TEO	$MoSe_2$/PEDOT:PSS
$Cu_{0.005}Bi_{0.5}Sb_{1.495}Te_3$	PCBM	PEDOT:PSS/ Si-NP
$Bi_{0.5}Sb_{1.5}Te_{2.7}Se_{0.3}$	CNTs/PANi	PDI-Te
$Bi_{0.48}Sb_{1.52}Te_3$+PbTe composite	PANi/PPy/SWCNT	Ni/PVDF
$(BiSbTe_{1.5}Se_{1.5})_{0.3}Ag_{0.3}$	CNT/PEDOT:PSS	NDINE/SWCNT
$Bi_2Te_{2.38}I_{0.02}Se_{0.6}$	PEDOT:PSS /RTCVD graphene	PDINE/SWCNT
	CNT/PVDF	

Recently, there has been a growing interest in reviewing TE materials, notably several excellent reviews on flexible TE materials [13,15-17], organic thermoelectric materials [18-19], and thermoelectric polymers [20-21]. In fact, each of these previous reviews has concentrated only on one type or one specification of TE materials at wide operating temperature range of 300 to 500 K. For example, Du et al. [13] reviwed the performance of only flexible TE materials, including inorganic, organic, and hybrid, but not the rigid ones. Therefore, less attention has been paid to study the efficiency of the three types of TE materials regardless of a certain specification. The purpose of the present paper is to provide a comprehensive overview of the most recently developed inorganic, organic and hybrid TE materials, and explore their efficiency at room temperature (300K). The paper is organized as follows. First, the TE efficiency basis is summarized in Section 2. Inorganic TE materials are reviewed in Section 3. The organic TE materials including polymer based TE composites and carbon based TE composites are illustrated in Section 4. The emerging topic of hybrid TE materials is covered in Section 5. The application of flexible TE materials in wearable TEGs is explained in Section 6. Furthermore, the conclusions and outlook are presented in Section 7.

2.   Thermoelectric efficiency

For an ideal TEG with constant thermoelecteric (TE) properties, the maximum heat-to-power conversion efficiecy (η_{max}) can be approximated by the following equation [22]:

$$\eta_{max} = \left(\frac{T_H - T_C}{T_H}\right) \cdot \left(\frac{\sqrt{1+Z\overline{T}} - 1}{\sqrt{1+Z\overline{T}} + \frac{T_C}{T_H}}\right) \tag{1}$$

where the conversion efficiency (η_{max}) is given as the ratio of temperature gradient between hot (T_H) and cold (T_C) reservoirs and the figure of merit $Z\overline{T}$ (the effective ZT across ΔT). The term in the first parenthesis on the right hand side is the Carnot efficiency of the thermoelectric device. Figure of merit limits how efficiently a TE material can convert thermal energy into electerical energy and is expressed as:

$$Z\overline{T} = \frac{(\alpha^2 \sigma T)}{\lambda} \tag{2}$$

where α is the Seebeck coefficient (μV/K), σ is the electrical conductivity (S/cm); T is the absolute temperature (K) and λ is the thermal conductivity (W/m K).

The numerator, $\alpha^2\sigma$, is called the power factor (PF). The $Z\overline{T}$ of the TE materials is higher when the thermal conductivity is low and the electrical conductivity and Seebeck coefficient are high. For this reason, researchers try to develope a TE material with high power factor, but low thermal conductivity. However, these material properties have trade-off relationships, which hinders the enhancement of $Z\overline{T}$ value [15]. For example, the Seebeck coefficient and electrical conductivity follow an opposite trend as a function of the carrier concentration. To put it another way, an increase in the carrier concentration leads to a decrease in the Seebeck coefficient, while improves the electrical conductivity [23]. Obviously, increasing the carrier concentration also increases the thermal conductivity, which is not desirable. In total , it is very difficult to individually tune one parameter without affecting another. As such, it is of critical importance to understand the TE properties and efficiency of each type of TE materials at room temperature regarding their fabrication methods and input raw materials.

3.   Inorganic TE materials

Conventional TE materials are mainly composed of inorganic compounds, including bismuth telluride (Bi_2Te_3) and its alloys, Lead telluride (PbTe) and its alloys, silicon-germanium (SiGe) alloys, antimony telluride (Sb_2Te_3), and tin selenide (SnSe) [24].These inorganic TE materials, especially Bi_2Te_3 , SiGe and PbTe, have been established in the early boom of thermoelectric research in 1950 ~ 1960s [5]. Until mid-1990s, the highest $Z\overline{T}$ value of the developed inorganic TE materials was remained close to unity, which was not cost-effective in most applications [21]. However, advances in science and technology and awareness of fossil fuels threats

provided a great willingness to improve the performance (as measured by $Z\overline{T}$) of the TE materials [23] .

Accordingly, since mid-1990s, research in the TE field has largely focused on enhancing TE properties of the inorganic TE materials through improving their Seebeck coefficient and thermal conductivity [13, 25]. Since 1950s, Sb_2Te_3, Bi_2Te_3, Bi_2Se_3 and their alloys are the most promising inorganic TE materials for operation at room temperature (300–400K) [26-27]. However, the abundancy of tellurium (Te) in the earth's crust is only around 0.001 ppm, which is even much less than that of gold (Au) with 0.004ppm [28]. Therefore, it is necessary to research for superb alternatives, which benefit from being Te free and performing efficiently at room temperature. In this regard, MgAgSb has attracted extensive attention owing to its lower cost, less toxicity, higher thermal stability, and lower thermal conductivity compared with Bi_2Te_3 alloys [29]. Although the focus of this paper is on the performance of TE materials at room temperature, but it should be noted that another motivation for replacing Bi_2Te_3 with MgAgSb is that the performance of Bi_2Te_3 degrades at temperatures over 373K [30]. This degradation is related to the small band gap of Bi_2Te_3, which subsequently results in a strong bipolar effect at high temperatures [31]. In what follows, the employed methods to improve the ZT of different inorganic TE materials will be discussed. In addition, Table 2 exhibits the summary of the TE properties of some inorganic TE materials at room temperature.

Table 2. The summary of the TE properties of some typical inorganic TE materials at 300K.

Type	TE material	α [μV/K]	σ [S/cm]	PF [μW/mK^2]	λ [W/mK]	ZT	Ref
P type	$Sb_{1.85}In_{0.15}Te_3$	124	500	-	0.9	0.27	[26]
	$Mg_{0.995}Li_{0.005}Ag_{0.97}Sb_{0.99}$	200	588	2300	0.9	0.75	[28]
	$Mg_{0.97}Zn_{0.03}Ag_{0.9}Sb_{0.95}$	85	952	690	1.25	0.28	[29]
	$MgAg_{0.97}Sb_{0.985}B_{0.005}$	255	285	1860	0.8	0.7	[31]
	$Bi_{0.38}Sb_{1.62}Te_3 + Ge_{0.5}Mn_{0.5}Te$	194	1100	43	1.28	1.22	[32]
	$CuInTe_2 + Bi_{0.4}Sb_{1.6}Te_3$	175	1250	40	1.1	1.15	[33]
	$Bi_{0.4}Sb_{1.59}Ge_{0.01}Te_3$	207	909	48	1.05	1.36	[34]
	$Cu_{0.005}Bi_{0.5}Sb_{1.495}Te_3$	150	1400	-	1	0.97	[35]
	$Bi_{0.5}Sb_{1.5}Te_{2.7}Se_{0.3}$	109	1250	-	0.96	0.48	[36]
	$Bi_{0.35}Sb_{1.65}Te_3$	270	285	-	0.9	0.8	[37]
	$Bi_{0.48}Sb_{1.52}Te_3 + 0.05wt\% PbTe$	177	1800	56	1.85	0.9	[38]
	$Bi_{0.4}Sb_{1.6}Te_3$ alloys +5 wt% Te	155	880	21	1.4	0.48	[39]

	$(BiSbTe_{1.5}Se_{1.5})_{0.3}Ag_{0.3}$	200	120	480	0.6	0.25	[40]
	$Bi_{0.8}Sb_{1.2}Te_3$	150	300	-	-	0.58	[41]
	$Mg_{0.995}Yb_{0.005}Ag_{0.97}Sb_{0.99}$	220	476	2180	0.81	0.8	[42]
	$MgAg_{0.97}Sb_{0.99}$	170	580	1620	0.8	0.55	[43]
	$MgAg_{0.97}Sb_1$	220	476	2280	0.88	0.78	[44]
	$Mg_{0.995}Ca_{0.005}Ag_{0.97}Sb_{0.99}$	225	416	2080	0.84	0.75	[45]
	$Mg_{0.97}Zn_{0.03}Ag_{0.9}Sb_{0.95}$	285	166	1250	0.62	1.1	[46]
	$Bi_{0.5}Sb_{1.5}Te_{3.2}$	224	800	-	0.65	1.2	[47]
N type	$Bi_2Te_{2.39}Se_{0.6}$	-160	1200	31	1.3	0.7	[48]
	Bi_2Se_3	-105	526	575	1.2	0.14	[49]
	$Bi_2Te_{2.7}Se_{0.3}$	-263	250	-	0.79	0.76	[50]
	$Bi_2Te_{2.7}Se_{0.3}$	-146	2250	49	2.09	0.81	[51]
	$Bi_2Te_{2.7}Se_{0.3}$ + 0.3 wt% KI	-135	1350	26	1.45	0.51	[52]
	Bi_2Te_3	-105	1600	17.5	1.65	0.33	[53]
	$Bi_2Te_{2.7}Se_{0.3}$	-168	600	1650	0.73	0.68	[54]

3.1. P type inorganic TE materials

In recent years, several strategies are adopted to raise the $Z\overline{T}$ values of TE materials such as optimizing carrier concentration, manipulating the band structure, nanostructure engineering, and manipulating the defects .In the meantime, $(Bi, Sb)_2(Se,Te)_3$-based alloys developed in the 1950s are the most popular inorganic p type TE materials at near- room temperature [55]. Thus, so far several efforts have been conducted to improve their TE performance, including optimizing carrier concentration [37], decreasing the lattice/bipolar thermal conductivity [56], incorporating a proper second nanophase [57, 58]. Duan et al. [32] tried to tune lattice thermal conductivity and mechanical property of $Bi_{0.38}Sb_{1.62}Te_3$ alloys by incorporating $Ge_{0.5}Mn_{0.5}Te$ into it. The work considered four stoichiometric ratio of 0, 0.5%, 1%, and 1.5% for $(Bi_{0.38}Sb_{1.62}Te_3)_{1-x}(Ge_{0.5}Mn_{0.5}Te)_x$ composite. The results exhibited that adding $Ge_{0.5}Mn_{0.5}Te$ to $Bi_{0.38}Sb_{1.62}Te_3$ alloys enhanced the carrier concentration, resulting an improvement in the Seebeck coefficient, but not the electrical and thermal conductivity, as shown in Figs. 3a-c. Then, the authors proposed to tune the carrier concentration by incorporating $BiCl_3$. The results indicated that 1% $BiCl_3$ reduced the carrier concentration and reached the minimum lattice thermal conductivity. Furthermore, incorporating 1% $BiCl_3$ improved both electrical conductivity and Seebeck coefficient of the composite. The authors concluded that at 300K,

the most optimal $Z\overline{T}$ value of 1.22 was achieved for $Bi_{0.38}Sb_{1.62}Te_3$ + $Ge_{0.5}Mn_{0.5}Te$ +1% $BiCl_3$ composite.
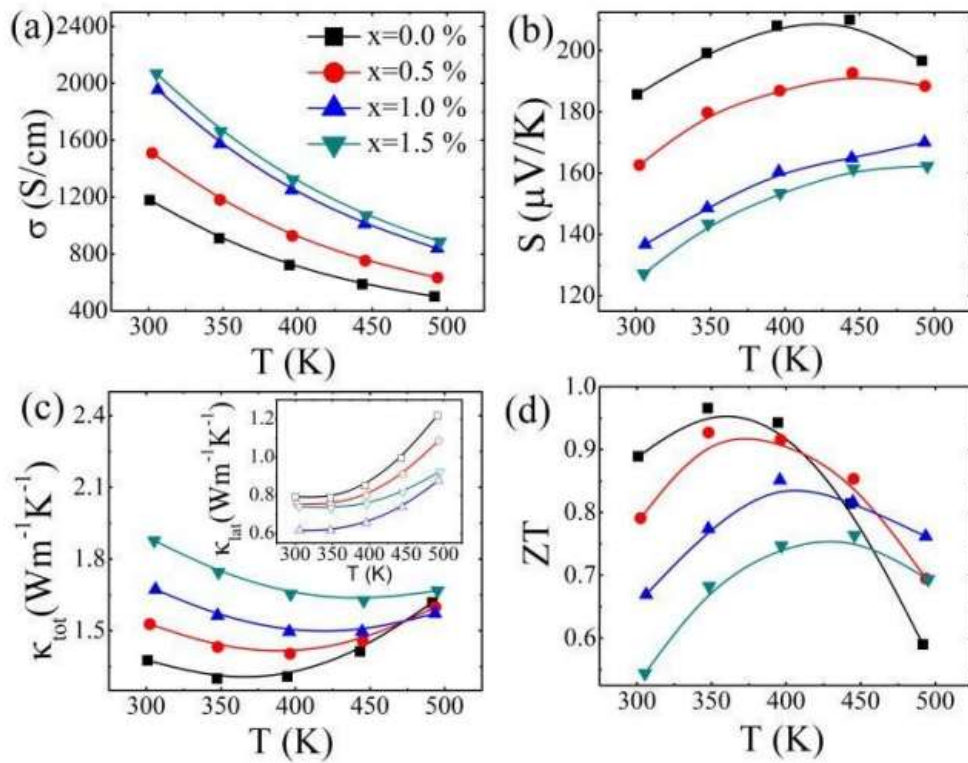
Fig. 3. Thermoelectric properties of $Bi_{0.38}Sb_{1.62}Te_3$ + x $Ge_{0.5}Mn_{0.5}Te$ (x = 0, 0.5%, 1%, and 1.5%): electrical conductivity (a), the Seebeck coefficient (b), thermal conductivity (c) with an inset of lattice thermal conductivity and $Z\overline{T}$ (d) [32].

Among several high pressure techniques to fabricate TE materials, including hot press, spark plasma sintering, extrusion methods and high-pressure synthesis, Wang et al. [33] investigated the TE performance of $Bi_{0.4}Sb_{1.6}Te_3$ alloys incorporated with $CuInTe_2$ inclusions using hot pressing method. The $CuInTe_2$ and $Bi_{0.4}Sb_{1.6}Te_3$ powders were mixed with the weight ratios of 0.1, 0.2, and 0.3%. Results showed that adding $CuInTe_2$ to $Bi_{0.4}Sb_{1.6}Te_3$ increased $Z\overline{T}$ value of the composite sample due to the increased hole concentration and phonon scattering. The authors illustrated that enhancement of hole concentration and phonon scattering in the $CuInTe_2$ /$Bi_{0.4}Sb_{1.6}Te_3$ sample led to higher electrical conductivity and lower thermal conductivity, respectively. Finally, the study reported that at 300K, 0.2% was the optimal weight ratio of $CuInTe_2$ /$Bi_{0.4}Sb_{1.6}Te_3$ with the maximum $Z\overline{T}$ value of 1.15, which was 12% higher than that of the pristine $Bi_{0.4}Sb_{1.6}Te_3$ sample.

For selecting an appropriate dopant, electronegativity of the replaced element should be taken into consideration. Thus, Wang et al. [34] used germanium (Ge) to substitute Sb in $Bi_{0.4}Sb_{1.6}Te_3$ alloys. The work focused on four Ge contents (x=0.00, 0.01, 0.015, 0.02) to achieve the nominal composition of $Bi_{0.4}Sb_{1.6-x}Ge_xTe_3$. The bulk samples were obtained by hot pressing of $Bi_{0.4}Sb_{1.6-x}Ge_xTe_3$ powders. The results show that Ge doping increases the electrical conductivity due to an increase in the hole concentration, but decreases the thermal conductivity attributed to the enhanced phonon scattering. Importantly, at room temperature (300K), $Z\overline{T}$ achieved its maximum value of 1.36 with $Bi_{0.4}Sb_{1.59}Ge_{0.01}Te_3$ sample, while obtained the minimum value of 0.8 with $Bi_{0.4}Sb_{1.58}Ge_{0.02}Te_3$ sample. Therefore, the authors demonstrated that although Ge doping enhanced the TE properties of pure $Bi_{0.4}Sb_{1.6}Te_3$, but it should be limited to a specific amount.

In terms of spark plasma sintering, Chiu et al. [26] studied the effect of this method on TE properties of polycrystalline $Sb_{2-x}In_xTe_3$ where x was in the range from 0 to 0.2 with 0.05 interval. The authors explained that in spite of the positive effect of high sintering temperature and pressure on the electrical conductivity, it deteriorated the Seebeck coefficient and increased the thermal conductivity. The work recommended that the optimal sintering temperature was at which Seebeck coefficient started degradation. Furthermore, the proper sintering pressure was at which the electrical conductivity to thermal conductivity ratio reached the maximum value. Accordingly, the most efficient sample at 300K was $Sb_{1.85}In_{0.15}Te_3$ with $Z\overline{T}$ value of 0.27. Likewise, Hao et al. [35] used spark plasma to synthesize $Bi_{0.5}Sb_{1.5}Te_3$ with copper (Cu). The study aimed to decrease the minor carrier density of $Bi_{0.5}Sb_{1.5}Te_3$ and its associated negative effects on the TE performance. The authors obtained 12 mm height cylinder shape $Cu_xBi_{0.5}Sb_{1.5}Te_3$ (x = 0.005, 0.01, 0.015) compositions using spark plasma sintering. It was observed that Cu doping improved the hole concentration and mobility of $Bi_{0.5}Sb_{1.5}Te_3$ materials, which ultimately improved the electrical conductivity, as shown in Fig. 4a. Conversely, Cu addition reduced the lattice thermal conductivity of the composites, see Fig. 4b, owing to the induced nanostructural defects. Combining lower lattice thermal conductivity and higher electrical conductivity, $Cu_{0.005}Bi_{0.5}Sb_{1.495}Te_3$ obtained the maximum $Z\overline{T}$ value of 0.97 at 300K, which was 27% higher than that of pristine $Bi_{0.5}Sb_{1.5}Te_3$ sample, as shown in Fig 4c.
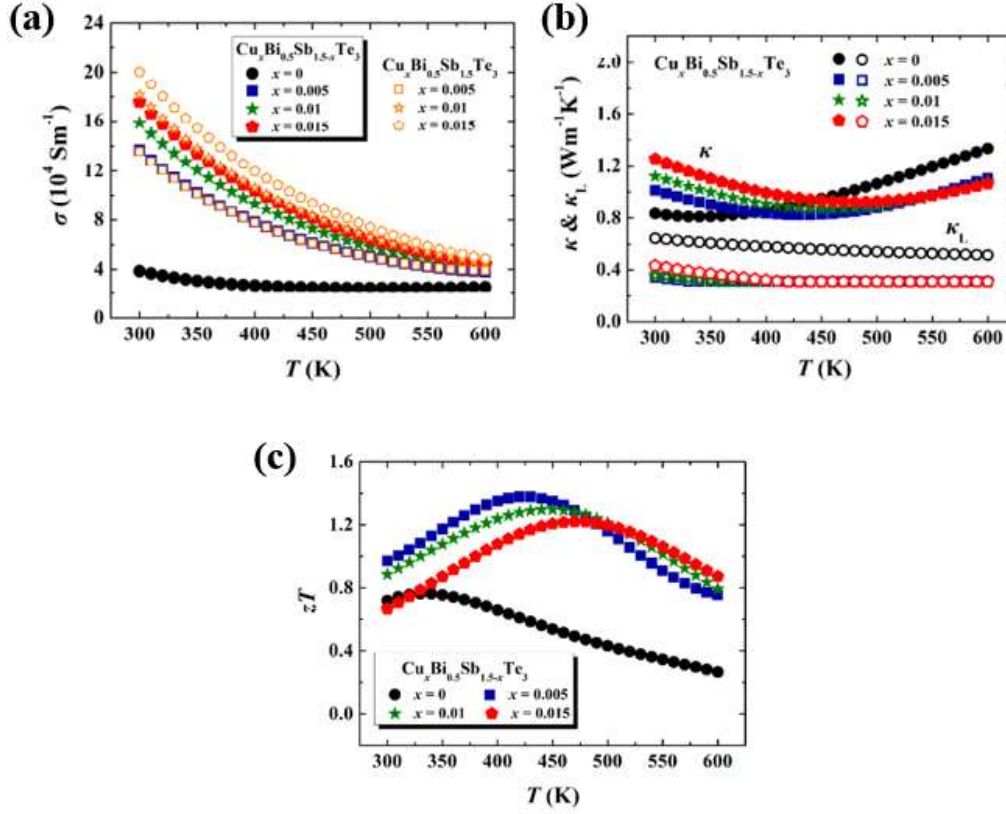
Fig. 4. Temperature dependences of (a) electrical conductivity σ and (b) total thermal conductivity κ (and lattice thermal conductivity κL) and (c) figure of merit $Z\bar{T}$ for nominal Cu-doped CuxBi0.5Sb1.5-xTe3 samples [35].

Instead of spark plasma method, Guo et al. [36] employed high pressure and high temperature method to synthesize $Bi_{0.5}Sb_{1.5}Te_{3x}Se_x$ alloys (x=0.3, 0.5 and 0.75). The results revealed that synthesis pressure and Se doping caused abundant distorted layers and lattice defects. Precisely, the lattice defects led to reduction in the thermal conductivity. Furthermore, increasing Se doping exhibited a directed relationship with both the electrical conductivity and Seebeck coefficient. The authors reported that the maximum $Z\bar{T}$ value of 0.48 is achieved at 300 K from the prepared $Bi_{0.5}Sb_{1.5}Te_{2.7}Se_{0.3}$ alloys.

Apart from high-pressure techniques, ball milling and melting are also the prevalent methods for preparation of bulk TE materials. Serrano-Sánchez et al. [37] synthesized Sb with Bi_2Te_3 compounds by arc melting method. The authors reported that arc melting minimized the thermal conductivity of the nominal $Bi_{2-x}Sb_xTe_3$ composition (x=1, 1.5, and 1.65), while maximized its electrical conductivity. This was primarily because of enhanced phonon scattering. The results showed that the highest concentration of Sb (1.65) led to the highest $Z\bar{T}$ value of 0.8 at 300K. In addition, Liang et al. [38] used the zone melting method to incorporate PbTe with $Bi_{0.48}Sb_{1.52}Te_3$ alloys with three different weight ratios of 0.05, 0.1, and

11

0.15wt%. Results revealed that although increasing the PbTe concentration remarkably decreased the lattice thermal conductivity of the $Bi_{0.48}Sb_{1.52}Te_3$+PbTe composite, but it had a tradeoff relationship with the Seebeck coefficient, as shown in Figs. 5a-b. Thus, the authors suggested to keep the PbTe content within 0.05 wt%, which resulted the optimal $Z\overline{T}$ of 0.9 at 300K, as Fig. 5c shows.
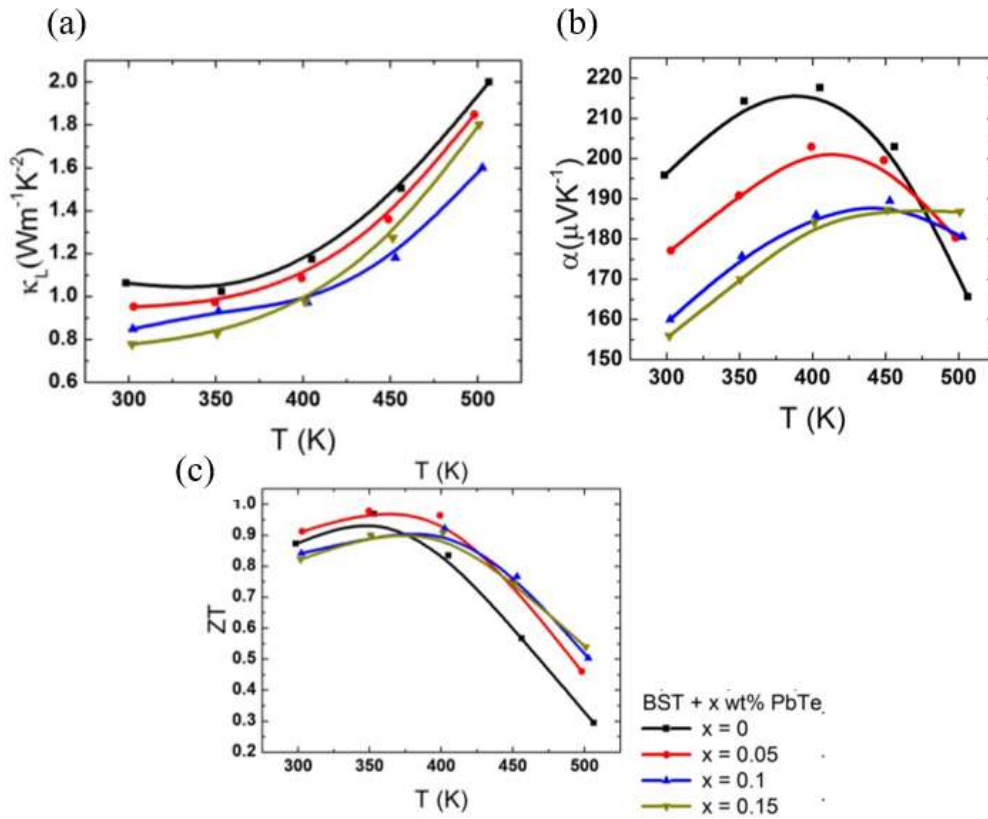
Fig. 5. Temperature dependences of (**a**) lattice thermal conductivity; (**b**) Seebeck coefficient; (**c**) figure of merit $Z\overline{T}$ for the $Bi_{0.48}Sb_{1.52}Te_3$ +x wt% PbTe samples [38] .

Liquid-state manipulation is another strategy for optimizing TE materials, which requires melting process. Gao et al. [39] employed liquid-state manipulation method to increase the TE properties of $Bi_{0.4}Sb_{1.6}Te_3$ alloys with 5 wt% Te. The authors claimed that the liquid state manipulation method raised the effective mass and carrier density, which consequently enhanced the Seebeck coefficient and the electrical conductivity, respectively. In addition, the samples prepared by this method exhibited greater phonons scattering, leading to a lower thermal conductivity. As a result, the highest recorded $Z\overline{T}$ at 300K was 0.48, which was 33% higher than that of the traditional melted $Bi_{0.4}Sb_{1.6}Te_3$ alloy.

Liquid phase compaction is another alternative , which optimizes the $\overline{ZT}$ value by minimizing the lattice thermal conductivity. Thus, Kim et al. [59] coupled spark plasma sintering with adding excess Te to compact the liquid phase of $Bi_{0.5}Sb_{1.5}Te_3$. The experiment was conducted by adding excess Te to the melt spun samples, followed by spark plasma sintering. The results showed that excess Te did not penetrate into the $Bi_{0.5}Sb_{1.5}Te_3$ ribbons, but covered the ribbons' entire surfaces. Furthermore, due to the spark plasma sintering, the excess Te expelled and formed dense dislocations in grain boundaries, which remarkably improved phonons scattering and maintained high carrier mobility. It is notable that the enhanced phonons scattering led to the reduction of the lattice thermal conductivity. The authors concluded that the obtained lower thermal conductivity, coupled with high carrier mobility, resulted in the maximum $\overline{ZT}$ value of 1.7 at 300K.

Likewise, Deng et al. [47] utilized both adding excess Te to the $Bi_{0.5}Sb_{1.5}Te_3$ composition and spark plasma sintering to control the chemical composition. The study demonstrated that the melt spun $Bi_{0.5}Sb_{1.5}Te_{3+x}$ (x=5,10,15,20,25) was spark plasma sintered (SPS) at 753K and a pressure of 70Mpa. Regarding the results, before spark plasma sintering, the extra Te distributed homogeneously at the boundaries of the melt spun $Bi_{0.5}Sb_{1.5}Te_3$ ribbon, but was not accommodated in it. In addition, the difference in Te-rich zone around the grain boundaries increased by increasing the Te content. This result revealed that due to the linear shape of $Bi_{0.5}Sb_{1.5}Te_3$ compound, any excess Te was segregated at the boundaries of $Bi_{0.5}Sb_{1.5}Te_3$ during melt spinning. Furthermore, the authors illustrated that after SPS, the excess Te was squeezed out, which resulted in rearrangement of grains and the creation of dislocations at the grain boundaries. Consequently, the lattice thermal conductivity and Seebeck coefficient greatly improved in parallel to the pressing direction. However, the authors reported that the highest $\overline{ZT}$ value was 1.2, which was obtained by samples with 25wt% excess Te in direction perpendicular to their pressing direction. This was because their electrical conductivity improved in this direction.

Although these methods for preparing TE materials have been effective to enhance the $\overline{ZT}$ of thermoelectric materials, but they are recognized with relatively complex processes. Therefore, Fan et al. [40] employed the high entropy alloys method to improve the TE properties of Bi_2Te_3 based bulk materials by adjusting their chemical composition. The experiment involved minor addition of silver (Ag), which is a prevalent dopant in the Bi_2Te_3-like compounds. The work

13

investigated the nominal composition of $(BiSbTe_{1.5}Se_{1.5})_{1x}Ag_x$, where x was equal with 0, 0.3, 0.6, 0.9 and 1.2 wt%, respectively. The results implied that severe lattice-distortion in the base $BiSbTe_{1.5}Se_{1.5}$ composite led to a low lattice thermal conductivity. In addition, minor incorporation of Ag further reduced the lattice thermal conductivity and improved the Seebeck coefficient of the composition. The authors reported that $(BiSbTe_{1.5}Se_{1.5})_{0.3}Ag_{0.3}$ obtained the peak $Z\overline{T}$ value of 0.25 at 300K, which was almost 66% higher than that of base $BiSbTe_{1.5}Se_{1.5}$ sample. In addition, Bochentyn et al. [41]introduced a new technique to synthesize $Bi_{2-x}Sb_xTe_3$ (x= 1.2, 1.6). The experiment started by Bi_2O_3, Sb_2O_3, and TeO_2 reagent grade oxides powders and continued by melting them in a ceramic crucible and quenching the melts. The bulk samples next grounded and pressed uniaxially to yield either $Bi_{0.4}Sb_{1.6}Te_3$ or $Bi_{0.8}Sb_{1.2}Te_3$ pellets. The authors incorporated hydrogen reduction technique at either 613K or 673K after milling the powders. The results indicated that at 300K, dehydronized $Bi_{0.8}Sb_{1.2}Te_3$ at 613 K achieved the optimal $Z\overline{T}$ of 0.58. This is mostly because of higher Seebeck coefficient of $Bi_{0.8}Sb_{1.2}Te_3$-613 (150μV/K) compared with that of the other samples.

As aforementioned, due to scarcity of Te element, which is used in the Bi_2Te_s alloys, MgAgSb has been introduced as a promising substitute at room temperature. However, there are two main issues facing the extensive progress of MgAgSb. First, the difficulty for synthesizing the pristine MgAgSb [43]. Second, the high electrical resistivity of an undoped MgAgSb attributed to its low carrier concentration. To address these issues, so far several efforts have been conducted to increase the carrier concentration using doping method. Liu et al. [28] doped Li (lithium) into Mg site to tune the carrier concentration. Accordingly, the nominal composition of $Mg_{1-x}Li_xAg_{0.97}Sb_{0.99}$ (x= 0, 0.0025, 0.005, 0.01, 0.02, and 0.04) was prepared by employing two-step ball milling and hot pressing processes. The results showed that at room temperature, there was a direct relationship between enhancing the electrical conductivity of the compound and increasing the Li content up to 2wt%. This was mainly because of increasing the carrier concentration. However, when the Li content exceeded the 2wt% of the compound, its impurity caused a reverse effect on the electrical conductivity of the compound. With regard to the Seebeck coefficient, doping Li deteriorated the Seebeck coefficient due to the bipolar effect originated from the small band gap of MgAgAb. In addition, increasing the Li concentration led to higher thermal conductivity of the compound, mainly due to the enhanced contribution of the electronic thermal conductivity. Consequently, the authors reported that at room temperature, the Li content should be limited up to 1wt% of the compound to achieve higher

$Z\overline{T}$ values than undoped MgAgSb. Precisely, the optimal Li concentration at room temperature was recorded to be 0.005, which resulted in the maximum $Z\overline{T}$ value of 0.75.

However, in a later study, Liu et al. [42] doped ytterbium (Yb) on the Mg site to enhance the carrier concentration of MgAgSb, and simultaneously created strong point-defect phonon scattering. The authors prepared the nominal composition of $Mg_{1-x}Yb_xAg_{0.97}Sb_{0.99}$ (x= 0, 0.0025, 0.005, and 0.01) by the two –step ball milling and hot pressing processes. The results delivered that at 300K, doping Yb increased the thermal conductivity due to bipolar effect. Likewise, the Seebeck coefficient deteriorated upon Yb doping, which was attributed to the increased carrier concentration. Conversely, the increased carrier concentration improved the electrical conductivity, resulted in boosting the $Z\overline{T}$ value up to 1.14 order of magnitude compared with that of the pristine MgAgAb.

Zheng et al. [29] doped MgAgSb with zinc (Zn) by combining the ordinary planetary ball milling and spark plasma sintering processes. The work explored the nominal composition of $Mg_{1-x}Zn_xAg_{0.9}Sb_{0.95}$, where x was equal to 0- 5%. The results showed that adding Zn to MgAgSb reduced the impurities content of Sb and their grain size until the Zn content was kept ≤3%. To put it another way, up to 3% Zn doping improved the purity and crystallinity of MgAgSb. Therefore, at room temperature, the electrical resistivity of $Mg_{1-x}Zn_xAg_{0.9}Sb_{0.95}$ samples decreased by Zn doping (x≤ 3). In addition, Seebeck coefficient was improved in all doped samples compared with undoped MgAgSb sample. It could be inferred that Zn doping reduced the carrier concentration, which led to improvement of the Seebeck coefficient. The authors also demonstrated reduction in the thermal conductivity of the samples by increasing the Zn content. The paper concluded that the highest $Z\overline{T}$ value at 300K was achieved by $Mg_{0.97}Zn_{0.03}Ag_{0.9}Sb_{0.95}$ sample with 0.28.

Liu et al. [45] selected Calcium (Ca) to be doped on the Mg site to optimize carrier concentration and consequently the $Z\overline{T}$ value. The results showed that the electrical conductivity and the Seebeck coefficient of the nominal composition $Mg_{1-x}Ca_xAg_{0.97}Sb0.99$ (x= 0, 0.0025, 0.005, and 0.01) respectively reached its highest and lowest values with x=.0.01. This was primarily because increasing the Ca content increased the carrier concentration. With respect to the thermal conductivity, at room temperature, it was deteriorated by increasing the Ca content owing to the small band gap of MgAgSb and the associated bipolar effect. The

paper demonstrated that the optimal Ca content was 0.005, which led to the maximum $Z\overline{T}$ value of 0.75. Apart from improving the thermoelectric properties, Gao et al. [31] used the doping method to enhance the mechanical property of MgAgSb. Accordingly, the authors Boron doped MgAgSb on the Sb site to obtain the nominal composition $MgAg_{0.97}Sb_{0.99-x}B_x$ (x= 0, 0.005, 0.01, and 0.02). The results indicated that also Boron doping deteriorated the $Z\overline{T}$ value at room temperature, but strengthened the solution, resulting in the largely increase of the micro hardness value of MgAgSb.

Instead of doping method, Lei et al. [43] manipulated the SPS system to explore its effect on the TE properties of MgAgSb. The authors explained that varying the SPS condition was selected to target Ag vacancies and Mg point defects, which act as acceptors to generate hole carriers. Therefore, the SPS process was conducted at different temperatures and holding times. The results showed that the samples sintered at lower temperatures contained metallic impurities phases, such as Ag3Sb or Sb phase, which reduced the hole carrier concentration. This issue was solved at higher sintering temperatures. However, further increasing the temperature granted extra energy to atoms, which led to their easily migration in the sample, recombination, and disappearance of Ag and Mg vacancies. As a result, the authors demonstrated that at higher sintering temperatures, the carrier concentration decreased, while the carrier mobility increased. Furthermore, the work illustrated that carrier mobility decreased by increasing the sintering time due to the increased vacancies concentration. Whereas, the carrier concentration slightly increased by increasing the sintering time due to the element evaporation.

To enhance the $Z\overline{T}$ value of MgAgSb, Liu et al. [44] tried to enhance the Sb content. Therefore, the authors prepared nominal composition of $MgAg_{0.97}Sb_x$ (x=0.99, 0.9925,0.995, and1.00) by combining ball milling and hot pressing processes. The results showed that carrier concentration gradually increased from x=0.99 to 0.995 due to generation of Ag and Mg vacancies, but then slightly decreased due to the very minor Sb impurities. In general, the authors claimed that increasing the Sb content improved the electrical conductivity, but deteriorated the Seebeck coefficient and the thermal conductivity. Finally, the work concluded that at 300K, increasing the Sb content up to x=1.00 improved the $Z\overline{T}$ value up to 2 times compared with that of x=0.99.

3.2. N type inorganic TE materials

Despite the high performance of classical bismuth telluride)Bi_2Te_3(alloys around room temperature, n-type Bi_2Te_3 alloys suffer from limited application to harvest low temperature waste heat. This is mainly attributed to the intrinsically excited electron –hole pairs across the band gap, leading to additional bipolar thermal conductivity, reduced totoal Seebeck coefficient and low $Z\overline{T}$ at elevated temperatures. Hao et al. [48] proposed doping a tiny amount of excessive Te and I dopant as electron donors to reduce the negative effect of intrinsic excitation on the electrical and thermal transport of n-type $Bi_2Te_{2.4}Se_{0.6}$ alloys. The experiment focused on two n-type TE compounds, including $Bi_2Te_{2.4+\delta}Se_{0.6}$ (δ = 0, 0.01, and 0.02) and $Bi_2Te_{2.4-x}I_xSe_{0.6}$ (x = 0.01 and 0.02). The results showed reduction in minority carrier partial electrical conductivity in both Te excessive and I doped $Bi_2Te_{2.4}Se_{0.6}$ samples, resulting in lower bipolar thermal conductivity. The authors reported that at 300K, $Bi_2Te_{2.4}Se_{0.6}$ was superior regarding the thermal conductivity and the Seebeck coefficient, while $Bi_2Te_{2.38}I_{0.02}Se_{0.6}$ obtained the highest electrical conductivity, as shown in Figs. 6 a-c. In total, the Te-excessive $Bi_2Te_{2.39}Se_{0.6}$ sample obtained the optimal $Z\overline{T}$ of 0.7 at near room temperature, as shown in Fig 6d. However, due to the advantages of high pressure synthesizing, including lower reaction temperature and shifted reaction equilibrium, Kang et al. [49] employed this method for synthesizing Bi_2Se_3 alloys. Thus working pressures of 1 to 6 Gpa were considered for sintering. In this study, the obtained products from high pressure sintering were grounded and sintered into a dense pellet using spark plasma sintering method. The authors revealed that at 300K, the highest $Z\overline{T}$ value of 0.14 was achieved by the synthesized sample at 1Gpa pressure.
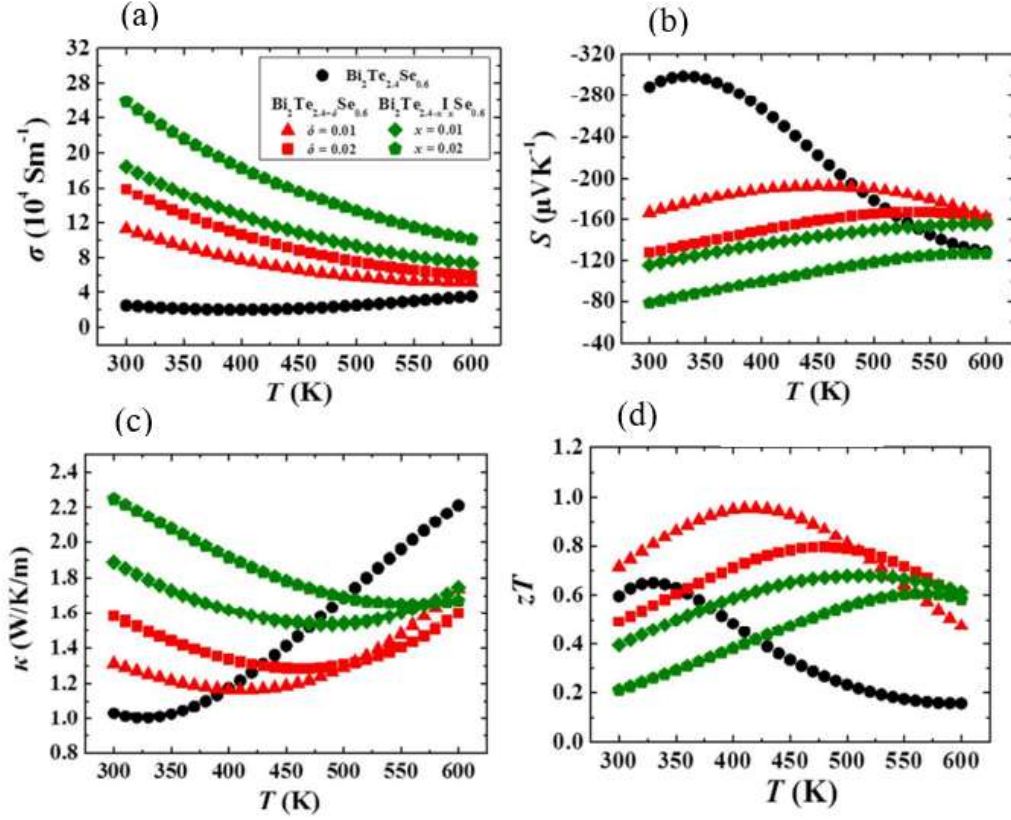
Fig. 6. Temperature dependences of (a) the electrical conductivity ; (b) Seebeck coefficient ; (c) thermal conductivity ; (d) figure of merit Z^-T for the $Bi_2Te_{2.4}+\delta Se_{0.6}$ (δ = 0, 0.01, and 0.02) and $Bi_2Te_{2.4}-xI_xSe_{0.6}$ (x = 0.01 and 0.02) samples [48] .

Nozariasbmarz et al. [50] tried to improve the TE properties of bulk nanostructured n-type $Bi_2Te_{2.7}Se_{0.3}$ materials using different techniques, including dopant addition, tellurium vacancies, glass inclusion, spark plasma sintering time and temperature, microwave processing, and subsequent annealing. The experiments were focused on optimizing the materials' properties concerning wearable TEGs. The results revealed that among different techniques, combination of microwave processing and re-spark plasma sintering resulted in the maximum $Z\overline{T}$ value of 0.76 at 300K. The authors explained that Se doping caused both power factor enhancement and thermal conductivity reduction, whereas microwave processing resulted in further enhancement of electrical conductivity and Seebeck coefficient.

Despite the advantages of re spark plasma sintering concerning TE properties improvement, it suffers from long processing time and sophisticated equipment. Therefore, Zhu et al. [51] suggested incorporation of liquid state manipulation method with direction solidified texturing to prepare $Bi_2Te_{2.7}Se_{0.3}$ bulk alloys. The results showed that liquid state manipulation remarkably raised the effective mass, resulting in a greater Seebeck coefficient. Whereas, high temperature-gradient directional solidification strengthened the texturing structure, leading to

18

a higher electrical conductivity. The authors concluded that at 300K, the optimal $Z\overline{T}$ value of 0.81 was achieved by $Bi_2Te_{2.7}Se_{0.3}$ after liquid state manipulation, which was 35% higher than that of an unexperienced liquid state manipulation sample. In addition, Zhu et al. [52] manipulated the liquid state (melting temperature) of $Bi_2Te_{2.7}Se_{0.3}$ alloys doped with 0.3 wt% potash iodide (KI). The results showed that due to the manipulation, microstructures and TE properties of $Bi_2Te_{2.7}Se_{0.3}$ + 0.3 wt% KI were changed remarkably. This was mostly because of the remarkable increase in the nanoparticles amounts and lattice defects, which leads to a great reduction in the thermal conductivity. The work concluded that at 300K, 0.51 was the maximum $Z\overline{T}$ of the composite, which was obtained with 750°C melting temperature.

However, Wang et al. [53] combined liquid state manipulation with subsequent ball milling and spark plasma sintering processes to improve the TE properties of Bi_2Te_3 alloy. The results revealed that thenliquid state manipulation increased both the carrier concentration and the effective mass of the composition, which surpassed the bipolar effect remarkably. Furthermore, the hierarchical microstructures attributed to the liquid state manipulation enhanced the multiscale phonon scattering, which reduced the lattice thermal conductivity by 43%. The authors concluded that the sample with liquid state manipulation exhibited maximum $Z\overline{T}$ value of 0.33 at 300K, which was slightly higher than that of without liquid state manipulation.

Comparing current fabrication methods, solvothermal synthesis provides better control over the size, structure, and morphology of the nanograins. However, this method lacks from time consuming process for removal of surfactants, which their existence effects the final TE performance. Therefore, Hong et al. [54] used microwave-assisted surfactant-free solvothermal method to synthesize $Bi_2Te_{3-x}Se_x$ within a short time. The experiments were conducted for nominal Se contents of 0.0, 0.1, 0.2, 0.3, 0.4, 0.5, 0.6, 0.7, and 1.0. Results showed that adding Se to Bi_2Te_3 alloy should be limited to 0.4wt%, since more Se concentration resulted in lower $Z\overline{T}$ value. Accordingly, at 300K, $Bi_2Te_{2.7}Se_{0.3}$ obtained the highest $Z\overline{T}$ value of 0.68, which was 23% higher than that of the conventional material. The authors explained that this higher $Z\overline{T}$ value is attributed to the established strong wide frequency phonon scatterings, increased optical energy gap, and the complex carrier scattering. Obviously, in spite of the extensive studies on improving the conversion efficiency of inorganic TE materials over the last decades, still $Z\overline{T}$ reaches the highest value of unity at room temperature. Besides, inorganic TE materials suffer from some inherent disadvantages, including a high cost of manufacturing, rarity, strong

toxicity, and processing difficulty [18]. Regarding wearable TEGs, they require to be flexible and stretchable to harvest waste heat from curvy surfaces of human body [60]. However, inorganic TE materials are inherently brittle and rigid that impedes their preparation in foldable and/or bendable films [13].

4. Organic TE materials

Organic thermoelectric materials, including polymers, carbon nanotubes (CNTs), and graphene [61], have been overlooked in the past decades attributed to their low $Z\overline{T}$ values and faster improvement of inorganic TE materials [62]. However, since organic TE materials get advantages of being inexpensive and recyclable [62], they may alleviate the aforementioned problems associated with inorganic TE materials [63]. In addition, due to the intrinsic flexibility of organic TE materials, such as conducting polymers, they have got attention for harvesting heat from human body as a non-planner heat source [64-66].

Performance of organic TE materials can be enhanced through either offering a new molecular design or fabricating nanocomposites comprise of conducting polymers or nanomaterials [21]. In general, organic TE materials possess low thermal conductivity (i.e. thermal conductivity of conducting polymers is 0.2–0.34 W/mK), which is difficult to further decrease [67]. Therefore, the ZT value of organic TE materials depends on the power factor (PF= $\alpha^2\sigma$), which can be enhanced by several orders of magnitude [20]. In this part, the recent advances in the TE performance of polymers and their corresponding organic composites such as carbon nanotubes and graphene are highlighted.

4.1. Polymer based TE material

There are two categories of polymers employed in organic thermoelectric materials, including conducting polymers and non-conducting polymers. Since the discovery of iodine- doped polyacetylene in 1977, conducting polymers have been used as electrode materials for rechargeable batteries [62]. Over the past few years, great efforts have been input to improve the PF of conducting polymers, including Poly(3,4-ethylenedioxythiophene (PEDOT), Polyaniline (PANI), and Polypyrrole (PPy), which possess the benefits of low thermal conductivity, non-toxicity and low cost [21]. Regarding non-conducting polymers, poly(3-octylthiophene), poly(3-hexylthiophene)(P3HT), and polyvinylidene fluoride are the most superior ones [18]. It is notable that due to the intrinsic electrical conductivity of conducting

polymers, they are the dominant polymers in majority of the thermoelectric device matrix compared with the non-conducting polymers. In addition, the non-conducting polymers act as a barrier for bundle-to-bundle hopping, which further decreases their thermoelectric performance [18]. The TE properties of some polymer based TE materials at room temperature are provided in Table 3.

Table 3. Summary of the TE properties of some typical polymer based TE materials at 300K.

Type	TE material	α [μV/K]	σ [S/cm]	PF [μW/mK^2]	Ref
P type	PEDOT:PSS films treated with H$_2$SO$_4$ and NaOH	39.2	2170	334	[67]
	PDPP3T doped with 6mM FeCl3/nitromethane	226	55	276	[68]
	PEDOT:S-PHE films	40	400	7.9	[69]
	PBTTT exposed to FTS vapor	33	1000	110	[70]
	PDTDE12 doped with F4TCNQ	80	75	20	[71]
	PDTDE12 doped with F4TCNQ	30	120	10	[72]
	PBDT-TT-TEO doped with F4TCNQ	190	1.3e-4	0.05	[73]
	C8TBT	60	2.2	1	[74]
	PEDOT:PSS post treated with TFMS–MeOH	21.9	2980	143	[75]
N type	FBDPPV doped with (N-DMBI)$_2$	-80	7.2	7	[76]
	PCBM doped with AOB and N-DMBI	-500	2	1	[77]
	P(PymPh) doped with NaNap	-16.4	18	0.485	[78]
	N-DMBI doped with A-DCV-DPPTT	-575	3.2	110	[79]
	PDPF doped with 5wt% N-DMBI	-235	1.3	4.65	[80]

4.1.1. P type TE polymers

Evidently, the electrical conductivity and Seebeck coefficient are interdependent. To illustrate, decreasing the charge concentration increases the Seebeck coefficient, but it decreases the electrical conductivity. However, improving the charge carrier mobility can enhance both the electrical conductivity and the Seebeck coefficient. Therefore, finding a strategy to enhance the charge mobility and adjust the carrier concentration is of importance for optimizing the TE performance of conducting polymers. Fan et al. [67] introduced sequential post-treatments using common acids and bases to precisely improve the charge transport and tune the doping level(carrier concentration) of PEDOT:PSS films. The experiments started by washing the PEDOT:PSS films with sulfuric acid (H$_2$SO$_4$) as an oxidization process, which enhanced the electrical conductivity remarkably, whereas increased the Seebeck coefficient slightly. Then,

the H2SO4-treated PEDOT:PSS films were treated with sodium hydroxide (NaOH) as a means to further enhance the Seebeck coefficient. These enhancements were attributed to the increased carrier mobility related to the acid treatment and the subsequent base treatment. The authors reported that the treated PEDOT:PSS films with H2SO4 and NaOH attained the highest PF of 334 µW/mK^2 at room temperature. Likewise, Jung et al. [68] proposed to increase both the electrical conductivity and the Seebeck coefficient by considering a high carrier mobility matrix and a small quantity dopant. Therefore, the authors used spin-coating to dope PDPP3T as one of the best performing conjugated polymer with FeCl3/nitromethane solution, which is a dopant. The results were compared with that of FeCl3/nitromethane doped P3HT. The authors indicated that higher carrier mobility of PDPP3T and lower level of dopant concentration enhanced the electrical conductivity and the Seebeck coefficient respectively, as shown in Fig. 8. Combining higher electrical conductivity and Seebeck coefficient, the highest PF was recorded for 6mM FeCl3/nitromethane doped PDPP3T with 276 µW/mK^2.
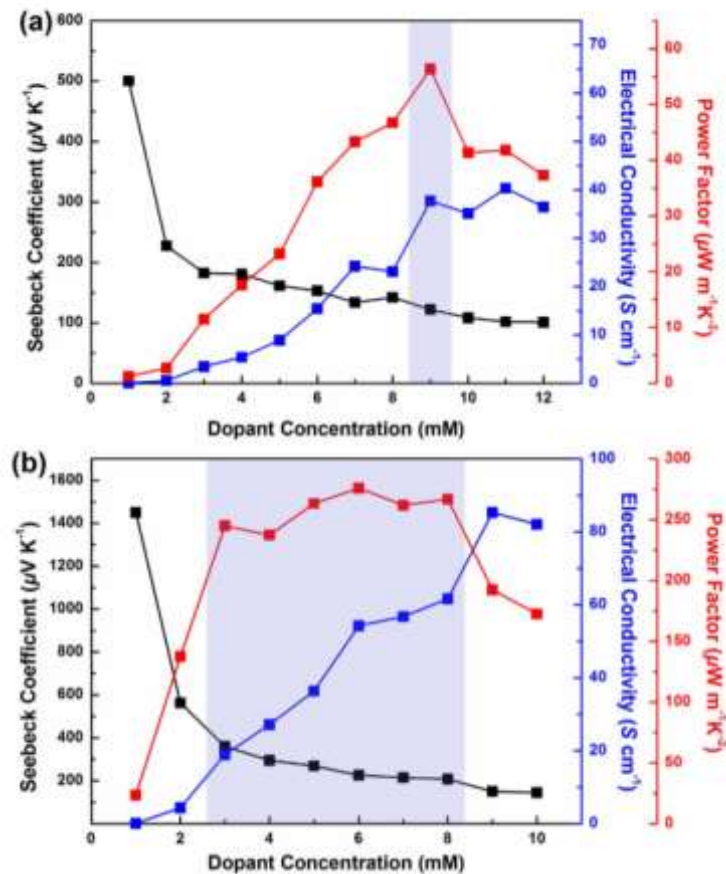
Fig. 8. Thermoelectric properties of (a) P3HT and (b) PDPP3T doped with FeCl3/nitromethane solutions by spin-coating [68].

The conducting polymers prepared by electrochemically polarization are flexible, free standing and mechanically strong. Zhang et al. [69] prepared flexible PEDOT:S-PHE films by constant-current polymerization of EDOT in propylene carbonate (PC) containing polymer electrolyte as a dopant, as shown in Fig. 9. The authors reported that decreasing the polymerization temperature or increasing the current density during polymerization increases both the electrical conductivity and the Seebeck coefficient of the PEDOT:S-PHE films simultaneously. Furthermore, the results showed that under the optimized polymerization conditions, the power factor of the prepared PEDOT:S-PHE films reached 7.9 $\mu W/mK^2$.
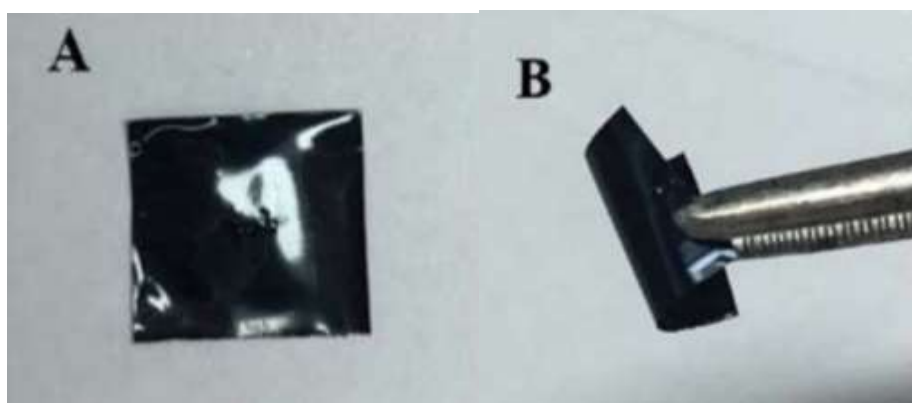
Fig. 9. (A) and (B) photos of PEDOT:S-PHE film [69].

It is notable that chemically or electrochemically doping of the semiconducting polymers generates charge carriers, leading to a higher electrical conductivity and strong structural perturbation changes. Therefore, it is difficult to predict the Seebeck coefficient of a semiconducting polymer doped chemically or electrochemically. Accordingly, Patel et al. [70] employed individually vapor deposition and immersion in an oxidative solution as the doping methods to accurately compare their influence on the PF value of a semiconducting polymer. The experiment focused on PBTTT as one of the high carrier mobility conjugated polymers. The results revealed that exposing the polymer to vapor of (tridecafluoro-1,1,2,2-tetrahydrooctyl) trichlorosilane (FTS) improved both the Seebeck coefficient and the power factor up to $33\mu V/K$ and $110\,\mu W/mK^2$, respectively. The authors highlighted that these values were almost two and four times higher than those of PBTTT immersed in a solution of 4-ethylbenzenesulfonic acid (EBSA).

Apart from the Seebeck coefficient, the doping method impacts on the morphological changes in the electrical conductivity. Lim et al. [71] employed vapor doping, which minimizes these morphological changes and makes it easier to study molecular doping in the semiconducting

polymers. The authors doped poly(3-hexylthiophene) (P3HT) thin films with F4TCNQ (small molecule) through vapor doping and compared its performance with that of the solution doped sample. It was reported that both doping methods resulted in almost the same Seebeck coefficient, but vapor doping led to a higher electrical conductivity. In total, the power factor of the vapor doped sample was by far higher than that of the solution doped sample. The authors concluded that the electrical conductivity of the films with the same dopant concentration can vary dramatically depending on the employed doping methods.

The effect of both dopant type and polymer structure on the PF was underlined in the work of Li et al. [72] .Thus, two p type polymers, including PDTDE12 film and PDTDES12 film, were doped by NOBF4 and F4TCNQ individually. The results revealed that there was an offset relation between the dopants' ratios and the Seebeck coefficient. Besides, the highest electrical conductivity was achieved with NOBF4-doped PQTS12. The authors explained that achieving high electrical conductivity was not mainly affected by carrier mobility of the pure polymer, but the dominant factor was the dopant type. Because the doping process could change the packing of bulk film and ultimately the charge transport, as shown in Fig. 10. The work reported that the highest PF was obtained by F4TCNQ-doped PDTDE12 with almost 10 $\mu W/mK^2$.
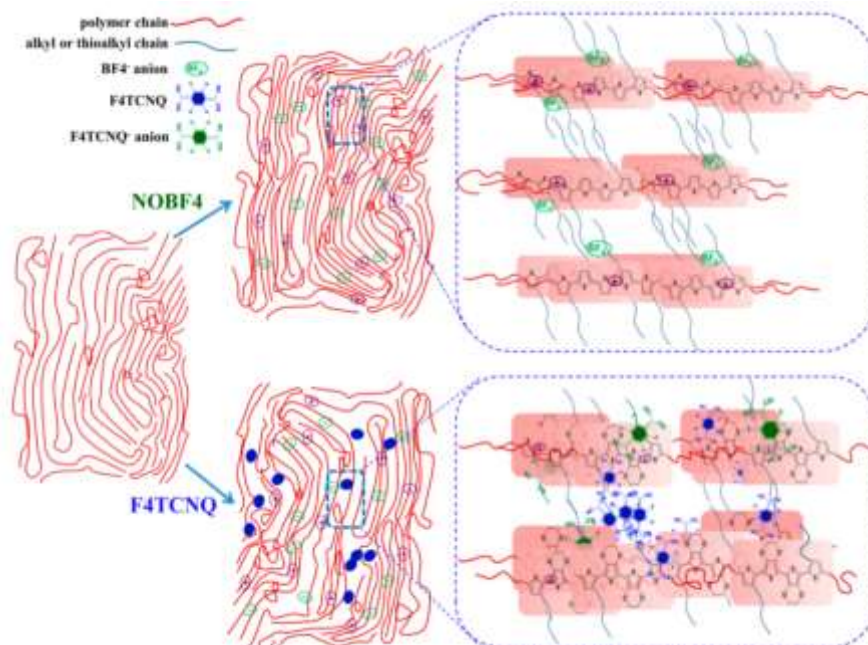
Fig. 10. Illustration of doping process and packing models doped by NOBF4 and F4TCNQ, respectively [72].

Conversely, Pan et al. [73] proved that the molecular structure of polymers also has a remarkable influence on the PF of polymers. The authors focused on the effect of polymer side chain on the thermoelectric performance of two benzo[1,2-b:4,5-b′]dithiophene (BDT)-based conjugated polymers. The considered polymers, including PBDT-TT with alkyl side chains and PBDT-TT-TEO with polar side chains, were doped with DDQ and F4TCNQ individually. The results confirmed that regardless of the dopant type, PBDT-TT-TEO with polar side chains obtained effectively greater power factor. This was because, the thermal stability of PBDT-TT-TEO decreased slightly due to containing polar side chains, which resulted in a niche increase in the band gap. As a result, after doping PBDT-TT-TEO with either DDQ or F4TCNQ, the polar side chains of PBDT-TT-TEO effectively reduced the clustering of the dopant molecules, leading to a significantly higher electrical conductivity and power factor compared with that of PBDT-TT. The authors reported that the highest power factors of PBDT-TT-TEO doped with DDQ and F4TCNQ were respectively 0.006 $\mu W/mK^2$ and 0.05 $\mu W/mK^2$ at 300K.

Likewise, Wang et al. [74] tuned the backbone structure of three donor-acceptor (D-A)-structured conjugated polymers, including F8BT, F8TBT, and C8TBT, to investigate its effect on their TE properties. Accordingly, the authors manipulated the polymers backbone structure by introducing fluorine and carbazole as electron-donor units, benzothiadiazole as electron-acceptor unit, and thiophene unit to tune the bandgap of polymers. The results revealed that C8TBT exhibited a higher power factor compared with that of F8TBT and F8BT. The authors attributed this higher PF to the formed thiophene and carbazole units in the polymer backbone, which enhance the molecular packing of the polymers.

The electrical conductivity and the Seebeck coefficient of the semiconducting polymer films also can be tuned by post treating with a mineral acid, which changes both the chain conformation and oxidation level of the polymer. Wang et al. [75] employed TFMS–MeOH as a post treatment solvent to improve the PF of PEDOT:PSS thin films. The results achieved from TFMS–MeOH post treatment were compared with those of two others post treatment solvents (such as DMSO, MeOH). The results showed that all the three types of post treatment solvents increased the electrical conductivity of the pristine PEDOT:PSS films, whereas the greatest increase was obtained by TFMS–MeOH post treatment. This was because, the TFMS–MeOH post treatment removed the insulating PSS parts and allowed the formation of a more densely packed and a higher degree crystalline structure, as shown in Fig 11. However, the work revealed that the Seebeck coefficient improved only by TFMS–MeOH post treatment,

since the Seebeck coefficient is inversely proportional to the carrier concentration and the carrier mobility. In total, the highest PF achieved by TFMS–MeOH post treatment was 143±15 $\mu W/mK^2$. Tomlinson et al. [81] utilized open shell TEMPO molecules as a charge neutral dopant to improve the electrical conductivity of P3HT without any converse effect on the Seebeck coefficient. The authors explained that using the open shell dopant improved the electrical conductivity independent of changing the oxidation state of the polymer.
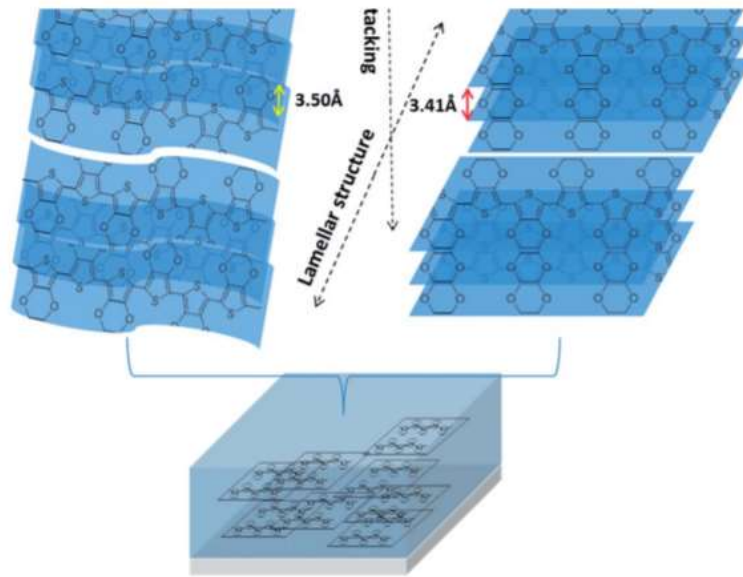
Fig. 11. The diagram of molecular structure arrangement of PEDOT film before and after TFMS–MeOH treatment. [75].

4.1.2. N type TE polymers

Tremendous efforts on solution-processable and air stable TE polymers have led to a remarkable improvement of p-type polymers over the last decades. Conversely, studies on n-type TE polymers still lag far behind because of their lower air stability, low solubility, and relatively low charge carrier mobility. To improve an n-type TE polymer regarding the requisite electrical conductivity, a suitable n -dopant can be utilized to directly transfer an electron to the host material. Therefore, the dopant creates additional charge carriers by reducing or oxidizing the n-type organic semiconductors.

Madan et al. [82] used sodium silica gel (Na-SG) particles as a reducing/doping agent to improve the TE properties of two different n type conjugated polymers, including NTCDI2DT-2T (N1) and NTCDI-AF4A (N2). The structures of these two polymers are shown in Fig. 12. The experiments were conducted for a varied weight percentage of Na-SG salts from a range

between 0 and 75wt% with 25% intervals. The results revealed that the 75 wt. % Na-SG doped NTCDI-AF4A and NTCDI-2T films achieved the average PF of 0.078 µW/mK^2 and 0.18 µW/mK^2, respectively. The authors attributed these higher PF to the three orders of magnitude higher electrical conductivity of the doped polymers compared with that of the pristine polymers.
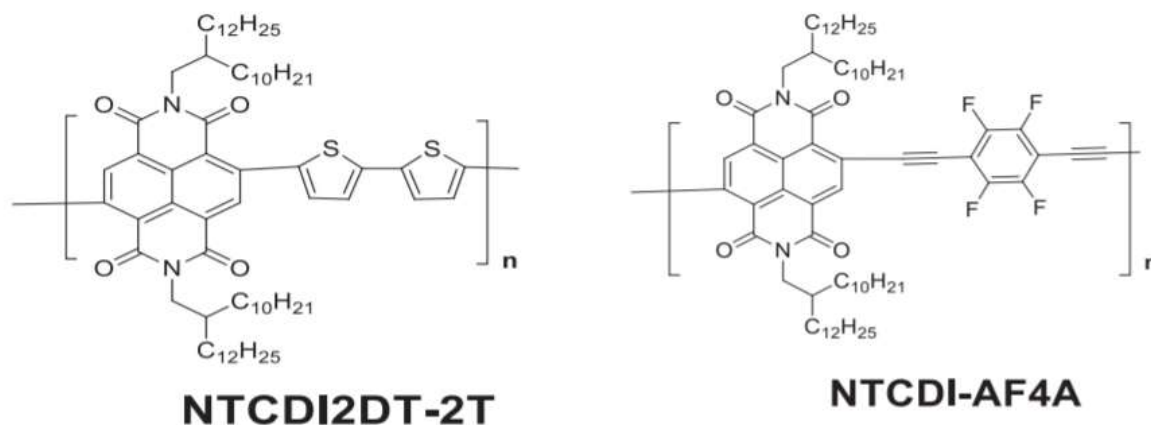
Fig. 12. Chemical structures of NTCDI2DT-2T (N1) and NTCDI-AF4A (N2) polymers [82].

Un et al. [76] explored the effect of dopant selection on the TE properties of FBDPPV. Three dopants, including (RuCp*mes)$_2$, (N-DMBI)$_2$, and N-DMBI-H used for n doping of FBDPPV. The results demonstrated that there is a converse relation between the dopant mol% and the Seebeck coefficient. Furthermore, among the three dopants, (N-DMBI)$_2$ doped FBDPPV yielded the best electrical conductivity of 8S/cm, and subsequently the highest PF of 7 µW/mK^2. Thus, the authors concluded that molecular dopants should contain more planar shape for less perturbation of the polymers microstructure. In addition, the molecular dopants should have clean and efficient pathways for electron transfer reaction. In spite of single doping, Gao et al. [77] codoped PCBM as a polymer with AOB and N-DMBI simoultanesly. Owing to the synergistic effects of AOB and N-DMBI, the electrical conductivity and the Seebeck coefficient of the codoped PCBM sample were higher than those of the single doped PCBM samples and unhoped PCBM samples. The results revealed that the maximum PF of 1.25 µW/mK^2 was reached when the dopant molar ratio was 0.11.

Although n-type conducting polymers that are soluble in organic solvents show high electron motilities, but they still need electron doping (reduction) to achieve the desirable electrical conductivity. Therefore, it is crucial to control the carrier density of n type polymers soluble in organic solvents. Hwang et al. [78] controlled the carrier density in solution processed polymer

P(PymPh) by changing the concentration of sodium naphthalenide (NaNap) as electron donor. The results showed that increasing the dopant concentration switched the semiconducting polymer from n type to p type operation. Furthermore, increasing the dopant concentration enhanced the electrical conductivity and power factor of the conducting polymer when it was in n-type operation. In particular, a maximum n-type power factor of 0.81 $\mu W/mK^2$ was demonstrated by 2.25 mM dopant.

Another fundamental factor affecting the TE performance of n-type polymers is their conjugated backbones structures. In fact, conjugated backbones structures determines the carrier mobility, the energy level, the charge transfer efficiency, and the carrier concentration of the doped materials. Huang et al. [79] studied the effect of the conjugated-backbone structure on the TE properties of two small molecules semiconductors, including A-DCV-DPPTT and QDCM-DPPTT. Accordingly, each of the determined semiconductors were doped by N-DMBI and the final solutions were spin coated on thin films. Results indicated that the conjugated-backbone structure of A-DCV-DPPTT allowed an efficient doping with N-DMBI, leading to the highest PF of 236 $\mu W/mK^2$, which was almost 48 order of magnitude higher than that of N-DMBI-doped Q-DCM-DPPTT. The authors attributed this higher PF to the higher electron mobility of A-DCV-DPPTT compared to that of Q-DCM-DPPTT. In a later study, Yang et al. [80] engineered the donor moiety of PDPF backbone, which is an n type DPP-based donor–acceptor (D–A) polymer. Then the engineered polymer was doped by N-DMBI in weight ratios of 2 to 17wt%. The results indicated that electron-withdrawing modification of the donor moiety of PDPF improved the electron affinity of the polymer and changed the polymer packing orientation. As a result, the highest PF value of 4.65 $\mu W/mK^2$ was achieved with 5% N-DMBI doped PDPF.

4.2. Carbon based TE composites

Carbon nanotubes (CNT) and graphene are the most widely used carbon materials as fillers in reinforced polymers nanocomposites [83]. There are four reasons why CNT and graphene have become so dominant. First, likewise conducting polymers, they intrinsically have high electrical conductivity. Second, their large specific surface area, as novel carbon nanomaterials, improves the interface between the polymer matrix and the carbon particles. Third, their high thermal conductivities are tunable through embedding them in the polymer matrix. Finally, they are flexible, low cost, non-toxic, lightweight, and contain high mechanical strength [18].

The TE properties of some carbon based TE composites at room temperature are provided in Table 4.

Table 4. Summary of the TE properties of some typical carbon based TE composites at 300K.

Type	TE material	α [μV/K]	σ [S/cm]	PF [μW/mK^2]	Ref
P type	SWNTs/PANI composite films	39	1440	217	[84]
	PPy/Graphene/PANi composite	28	500	52.5	[85]
	PANiPy/SWCNT composite	41	425	70	[86]
	CNT/PEDOT:PSS treated with Ethylene glycol	43.7	780	151	[87]
	SWNTs/ PEDOT: PSS treated with DMSO	42.5	500	105	[88]
	Alternate layers of PANi/graphene-PEDOT:PSS/PANi/DWNT-PEDOT:PSS	120	1800	2710	[89]
	PEDOT:PSS /RTCVD graphene composite film	54	193	56.28	[90]
N type	DWNT-PEI/graphene-PVP nanocomposites	-80	300	190	[91]
	SWNT film doped with PEI solution	-62	3500	1500	[92]
	SWCNT doped with PVA	-40	0.66	0.1	[93]
	CNT web doped with benzyl viologen (BV)	-120	2200	3103	[94]

4.2.1. *P type carbon based TE composites*

In recent years, it has been reported that the TE properties of organic materials could be enhanced through nanocomposites preparation [89,95-96]. Among them, (CNTs)/PANi composites are one of the most extensively studied type, which make a PANi interface layer on the surface of CNTs. In fact, the degree of ordering of the molecular chain arrangement has crucial effects on the TE properties of CNTs/PANi composites. Therefore, Wang et al. [84] studied the ordering of the PANi molecular chains in the SWNTs/PANI composite films through combining the in situ polymerization with solution processing. The results indicated that incorporating solution processing and in suite polarization methods both improved the dispersion of SWNTs in the composites and created stronger π- π conjugated interactions between PANi and the SWNTs. As a result, a highly ordered structure of PANi was prepared on the CNTs surface, which increased the carrier mobility and consequently enhanced the electrical transport properties of PANi. The work reported that the highest PF of the prepared SWNTs/PANi composite films reached 217 μW/mK^2 with 65% SWNTs content. Likewise, Wang et al. [85] utilized the same methods to form strong π-π interactions among Polypyrrole

(PPy), Graphene (GNs) and Polyaniline (PANi). The results demonstrated that both the in situ polymerization and solution process increased the homogeneous dispersion of GNs in PPy matrix, resulting in increased nanointerfaces in the PPy/GNs/PANi composite. In addition, combination of PPy with PANi with similar molecular chain structure led to more carrier mobility. The authors reported that the highest power factor was 52.5 $\mu W/mK^2$, which was obtained by the prepared PPy/GNs/PANi composite with 32% graphene concentration.

To improve the alignment of PANi molecular chain in PANi/SWCNT composite, Wang et al. [86] introduced polypyrrole (PPy), which is a well-known aligned polymer , onto the PANi backbone. The measurements revealed that a strong interaction was formed between the pyrrole and the aniline units on the random copolymer (PANiPy) backbone, as shown in Fig13 . The results indicated that PANiPy/SWCNT composites exhibited the highest power factor of 70 $\mu W/mK^2$ at 300K, which was by far greater than that of PANi/SWCNT, PPy/SWCNT, and PANi/PPy/SWCNT composites. This higher PF was because of an optimum balance between the electrical conductivity and the Seebeck coefficient of PANiPy/SWCNT.
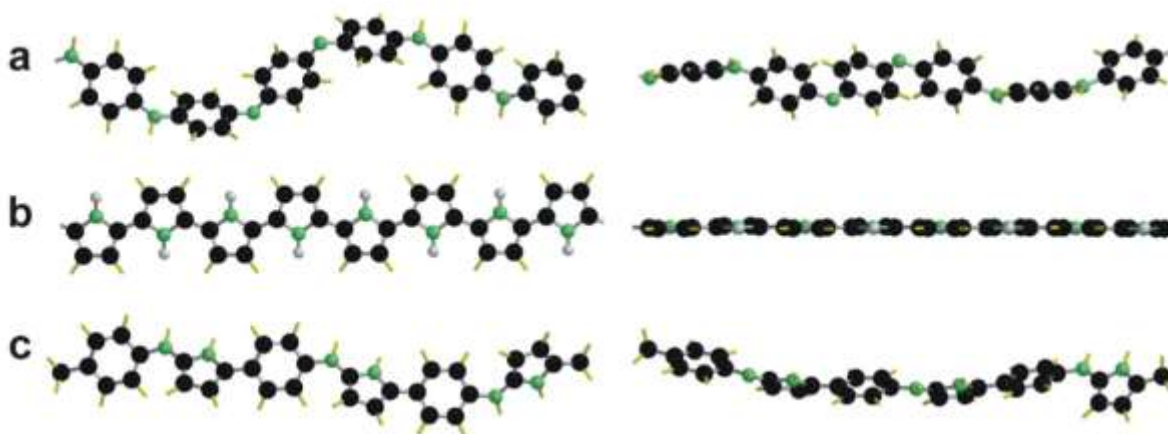
Fig. 13. Top view (left) and side view (right) of the partial chain segment conformation of PANi (A), PPy (B), and PANiPy (C) under the lowest energy state [86].

Another striking approach to enhance the electrical conductivity of organic nanocomposites is solvent treatment, which is dipping the organic films into Ethylene Glycol (EG), dimethyl sulfoxide (DMSO) or acid. Accordingly, Lee et al. [87] post treated CNT/PEDOT:PSS nanocomposite films with Ethylene glycol (EG). The 1hr immersed CNT/PEDOT:PSS nanocomposite films in EG were annealed at 140 °C for 10 minutes. The results revealed that treating the CNT/PEDOT:PSS nanocomposite films reduced the average inter-CNT bundle distance, leading to an increase in the electrical conductivity of the nanocomposite film. The

authors concluded that the EG treated nanocomposite films with 20 wt% CNT obtained the highest PF of 151 ± 34 μW/mK^2. Rather than EG, Jang et al. [88]utilized dimethyl sulfoxide (DMSO) to treat SWNTs/ PEDOT: PSS composite films. The experiment was conducted by mixing pristine PEDOT: PSS solution with 10mL DMSO containing SWNTs. Using DMSO as an organic solvent to disperse SWNTs improved the solubility of SWNTs. In addition, it enhanced the carrier mobility of PEDOT:PSS by conformational changing of the PEDOT chain and removal of nonconductive PSS. The authors reported that 60% SWNTs content resulted in the maximum power factor of 105 μW/mK^2 for the prepared flexible SWNTs/ PEDOT: PSS composite films.

Among the most important methods for preparation of polymer nanocomposites, such as direct mixing, in situ polymerization, sol gel process, melt intercalation, template synthesis, solution processing, and layer-by-layer assembly [97-98], Cho et al. [89] used LbL deposition process to assemble PANi, graphene, PEDOT:PSS, and DWNT. The layering was repeated in a range between 20 to 80 cycles, as shown in Fig. 14. The results revealed that the organic film comprised of an alternate layers of PANi/graphene-PEDOT:PSS/PANi/DWNT-PEDOT:PSS resulted in the maximum PF of 2710 μW/mK^2 with 80 cycles. The authors demonstrated that this higher PF is attributed to two reasons. First, improved carrier mobility in the interconnected and layered architecture of the conducting polymer, which was covered by DWNT. Second, the bridging between the graphene sheets. Conversely, an alternate layers of PANi/graphene-PEODT:PSS resulted in the minimum PF of 0 μW/mK^2.
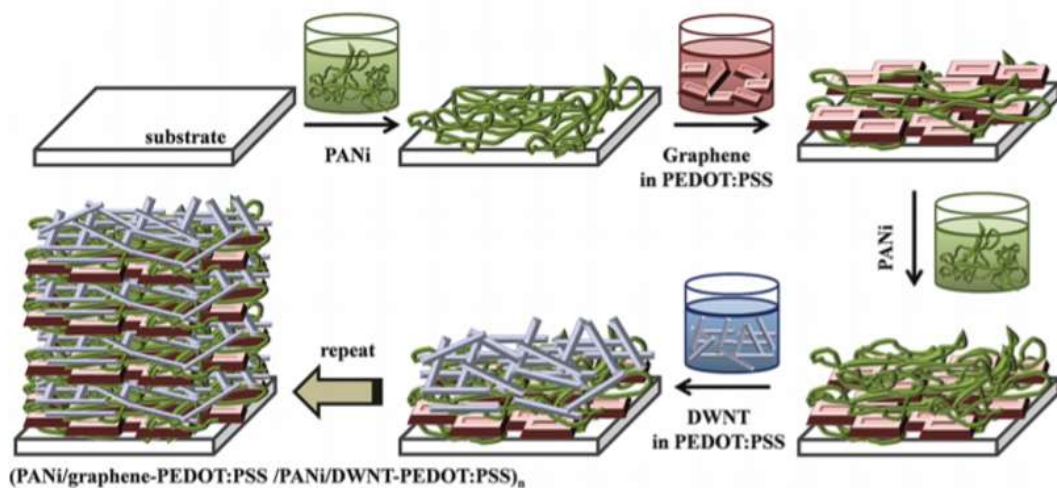
Fig. 14. Schematic of the layer-by-layer deposition process [89].

Solution based technique is the most common method to form carbon based polymer nanocomposites [99], and can be classified into spin coating, printing and spraying [100]. Park et al. [90] spin coated a rapid thermal chemical vapor deposition (RTCVD) graphene surface with PEDOT:PSS solution, as shown in Fig. 15. The experiment was conducted for spin rate of 500 to 5000 rpm. The results showed that the spin coating minimized the cracks and the defects on the RTCVD graphene surface, resulting in higher electrical conductivity. Furthermore, the Seebeck coefficient improved due to the high electron mobility attributed to the pep stacking interaction between the PEDOT:PSS backbone and the RTCVD graphene surface. The authors reported that while the pristine PEODT:PSS film reached the PF of 0.66 $\mu W/mK^2$, the PEDOT:PSS /RTCVD graphene composite film exhibited the maximum PF of 56.28m $\mu W/mK^2$ at 5000rpm.
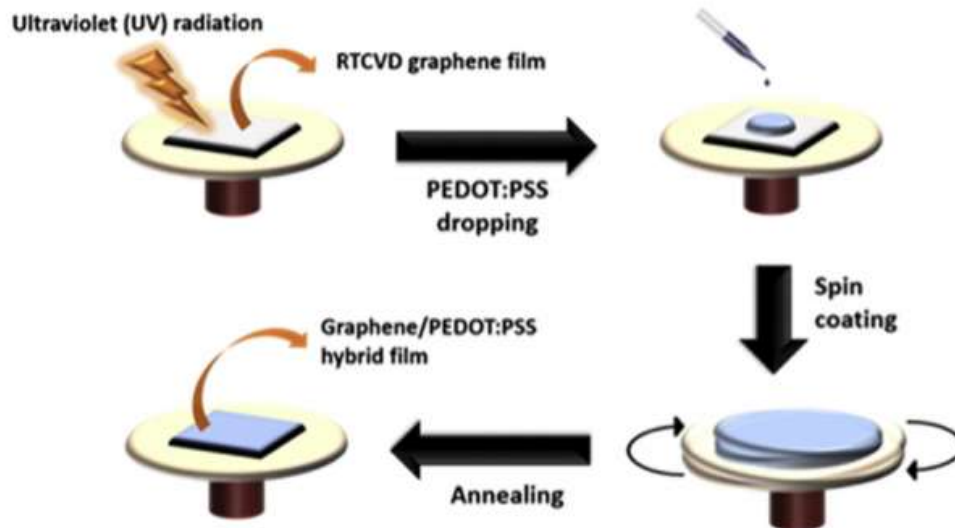
Fig. 15. Schematic illustrating the preparation of P/RTG hybrid films [90].

4.2.2. N type carbon based TE composites

Stable doping of the n-type organic TE films is the main challenge to overcome their lower power factor compared to that of the p-type counterparts. To put it another way, exposing the n-type TE composites in air turns their negative Seebeck coefficient into positive values. In addition, it is of critical importance to provide an opportunity to control the dispersion of nanoparticles in the polymer matric to provide a homogeneous thin film. In this regard, Cho et al. [91] utilized LbL method to generate an n type thin film by dipping the substrates alternately into the Graphene-PVP and DWNT-PEI solutions. The results revealed that the formed bridges between the graphene sheets and DWNT provided higher charrier mobility and ultimately a

32

greater Seebeck coefficient. The authors demonstrated that the parallel alignment of the graphene platelets on the substrates hindered the oxidization, which improved the air stability of DWNT-PEI/graphene-PVP nanocomposites. The results revealed that DWNT-PEI/graphene-PVP nanocomposites exhibited the highest power factor of 190 $\mu W/mK^2$ at room temperature.

To provide CNT/polymer composites, solution doping is the most striking approach to create n-type films. Montgomery et al. [101] spray doped the n-type PEI/DMF solution over the p type CNT/PVDF film. The solution dissolved the surrounding PVDF, and PEI infiltrated the CNT network. The results showed that, after DMF evaporation, the CNT/PVDF film altered to an n type TE composite with 10wt% CNT/PVDF and 0.1 mass ratio of PEI/CNT.

Since the n-type films are normally fabricated under air exposure, the effect of oxygen adsorption should not be undervalued. Zhou et al. [92] converted a p type SWNT film to an n-type film by drop-casting polyethyleneimine (PEI) solution. The results showed that the CNT bundles were coated by amine-rich PEI molecules, which increased the electron concentration. In addition, PEI coating deterred oxygen doping, which maintained the n type characteristics for a long period of 3 months. The authors reported that the prepared n type TE films achieved the highest power factor of 1500 $\mu W/mK^2$ with 1 wt.% PEI content. Likewise, Horike et al. [93] switched a p type SWCNT into an n type by polymer doping. Thus, four different polymer solutions, including poly(vinyl chloride) (PVC) , poly(vinyl pyrrolidone) (PVP), poly(vinyl alcohol) (PVA) and poly(vinyl acetate) (PVAc) were drop casted over p type SWCNT thin films as electron donors. The results revealed that the high occupied molecular orbital levels of the polymer and abundancy of oxygen in the polymer directly effect on the negative Seebeck coefficients of the SWCNTs. As the result, PVA with abundant oxygen obtained the highest Seebeck coefficient due to acting as both an electron donor and an oxygen barrier layer. To illustrate, the PVA doped SWCNT thin films with the highest Seebeck coefficient over 20 days' periods achieved the highest power factor of 0.1 $\mu W/mK^2$.

To fulfill the requirements of an n type organic TE composite, An et al. [94] fabricated a combination of n type dopants and annealing treatment. The experiments conducted with various n type dopants, including PEI, thiamin pyrophosphate (TPP), benzyl viologen (BV), and F4TCNQ. The results revealed that although adding a selective dopant resulted in a higher PF compared with that of the pristine CNT, but all doped CNT samples exhibited higher PF in conjunction with annealing treatment. This was dominantly because the annealing treatment removed oxygen from

33

CNT surface and made it more air stable. The authors illustrated that an annealed CNT web doped with benzyl viologen (BV) resulted in a maximum power factor of 3103 $\mu W/mK^2$, which was about 1.6 order of magnitude higher than that of a pristine CNT web treated with BV.

5.   Inorganic-organic (hybrid) TE composites

In spite of the tremendous efforts to improve the TE properties of pure inorganic and organic TE materials, their performances remain insufficient for fabrication in wearable TEGs. Precisely, the $Z\overline{T}$ of the organic TE materials is usually 2-3 times lower than that of the inorganic counterparts [102]. This is because organic TE materials contain lower electrical conductivity and Seebeck coefficient, resulting in lower power factors compared to those of inorganic TE materials.   However, organic TE materials benefits from low thermal conductivity, low density, low cost, low environmental impacts, and good mechanical flexibility [16]. As mentioned above, current TE materials possess $Z\overline{T}$ values less than 1, while the ambition is TE materials with $Z\overline{T}$ value 3 or greater. In order to obtain higher TE performance, such materials must have a high electrical conductivity and Seebeck coefficient, but low thermal conductivity. Therefore, achieving all these requirements in one TE material is of importance. Consequently, one striking strategy is to develop hybrid TE composites through combining classical inorganic and organic TE materials. Thus, hybrid TE materials can potentially conjoin the benefits of inorganic and organic TE materials. In what follow, recent works and development of hybrid TE materials are highlighted and summarized. The TE properties of some inorganic/organic TE composites at room temperature are provided in Table 5.

Table 5. Summary of the TE properties of some typical inorganic/organic TE composites at 300K.

Type	TE material	α [μV/K]	σ [S/cm]	PF [μW/mK^2]	Ref
P type	Te-PEDOT:PSS thin film	50	100	25	[103]
	PC-Te/PEDOT:PSS treated by H_2SO_4	75	250	141.9	[104]
	PC-Te/PEDOT:PSS treated by H_2SO_4	56	332	104	[105]
	Te–Bi_2Te_3/PEDOT:PSS treated by H_2SO_4	93.63	70	60.05	[106]
	Te NWs/PEDOT NWs	25	400	28	[107]
	Te- MWCNT/PANI	57.5	130	54.4	[108]
	Bi-Te based alloy nanosheet /PEDOT:PSS	21	1200	53	[109]
	SnSe nanosheets/PEDOT:PSS	100	300	390	[110]
	$MoSe_2$/PEDOT:PSS	21	1000	48.6	[111]

	PEDOT:PSS/ce-MoS$_2$	21.9	867	41.6	[112]
	PEDOT:PSS/ Si-NP	24	510	27.5	[113]
	Alternately Sb$_2$Te$_3$/CH3NH3I/ Sb$_2$Te$_3$ layers	300	170	1600	[114]
	Graphene nanosheets /Bi$_{0.4}$Sb$_{1.6}$Te$_3$	177	1428	4600	[115]
	CNTs/Bi$_{0.4}$Sb$_{1.6}$Te$_3$	180	1000	3200	[116]
	Bi$_2$Te$_3$/PEDOT:PSS	260	67	432	[117]
	MgAg$_{0.97}$Sb$_{0.99}$/CNTs	183	650	2200	[118]
N type	SWCNT dipped into KOH and 18-crown-ether	-33	2050	230	[119]
	Te nanowires/PDI	-310	1.6	18.6	[120]
	Ni/PVDF	-20	4500	200	[121]
	PP-CNT-CuO-PEG	-58	0.2	0.78	[122]
	PDINE/SWCNT	-46	500	112	[123]
	NDINE/SWCNT	-55	400	135	[123]
	SWCNT/ADTAb	-44.5	642.4	124	[124]
	TiS$_2$(TBA)$_{0.013}$(HA)$_{0.019}$	-140	450	904	[125]

5.1. P type hybrid TE materials

One of the most dominant approach for improving the performance of hybrid TE materials is incorporating nanostructured inorganics (i.e. Tellurium, Bi$_2$Te$_3$, CNT, and graphene) with conducting polymers [11]. In fact, this strategy shows a great promise for coupling high electrical conductivity and Seebeck coefficient of the nanostructured inorganics with low thermal conductivity of conducting polymers. Accordingly, Li et al. [103] drop casted PEDOT:PSS aqueous solution with Tellurium (Te) NWs ethanol solution and sonicated the mixture to prepare Te-PEDOT:PSS thin film. The results revealed that increasing the PEDOT:PSS more than 10wt% has a trade-off relationship with the power factor. Consequently, the maximum PF of the prepared Te-PEDOT:PSS thin film was 25 µW/mK^2 with 10wt% PEDOT:PSS concentration.

To improve the electrical conductivity, the insulated PSS chains could be removed from the surface of PEDOT:PSS film by post-treatment processing with concentrated H$_2$SO$_4$, H$_3$PO$_4$, or DMSO. Meng et al. [104] added Te (PC-Te) nanorod to PEDOT:PSS solution and post treated the mixture by H$_2$SO$_4$ to form PC-Te/PEDOT:PSS composite films, as shown in Fig. 16. The results revealed that the highest PF of 141.9 µW/mK^2 was obtained for the PEDOT:PSS:PC-Te film containing 90wt% PC-Te nanorods and treated with 12MH$_2$SO$_4$. In fact, this PF value

was 2.75 order of magnitude greater than that of untreated PEDOT:PSS:PC-Te film. The authors explained that without H_2SO_4 treatment, there was a direct relationship between the content of inorganic component and both the Seebeck coefficient and the electrical conductivity. However, H_2SO_4 treatment had a tradeoff relationship with the Seebeck coefficient, but a direct relationship with the electrical conductivity.
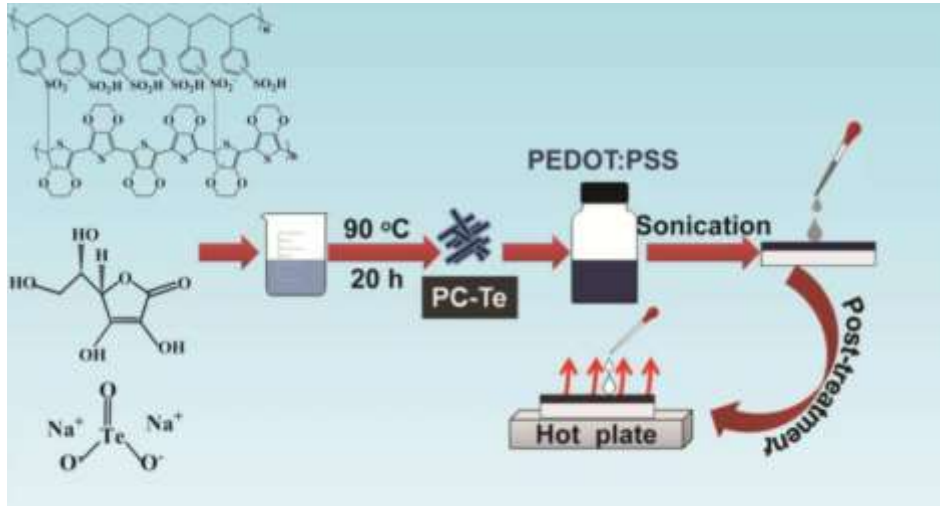
Fig. 16. Schematic illustrations of the fabrication and post-treatment of the composite films [104].

In a later study, Meng et al. [105] used Te (PC-Te) nanorad to coat SWCNT/PEDOT:PSS films. To conduct the experiment, Te (PC-Te) nanorad was added to SWCNT/PEDOT:PSS mixture and treated through a simple vacuum assisted filtration method. Then, H_2SO_4 was doped for post treating the SWCNT/PC-Te composite film, as shown in Fig. 17. The results displayed that although adding SWCNT to the mixture improved the electrical conductivity, but reduced the Seebeck coefficient of the composite film. Likewise, treating with H_2SO_4 enhanced the electrical conductivity, but reduced the Seebeck coefficient of the film remarkably. The authors concluded that the optimal PF was 104 μW/mK^2 for the composite film containing 70% SWCNT. Bae et al. [106] covered Te–Bi_2Te_3 nanowire heterostructures with PEDOT:PSS through a solution-phase reaction at a low temperature. The hybrid solution of Te–Bi_2Te_3/PEDOT:PSS was spray printed on a glass substrate to form a flexible thermoelectric generator. The results revealed that the acid treatment by H_2SO_4 increased the electrical conductivity of the hybrid film regarding the acid concentration. In total, 60.05 μW/mK^2 was the optimal PF achieved by 60 volume percent of H_2SO_4.
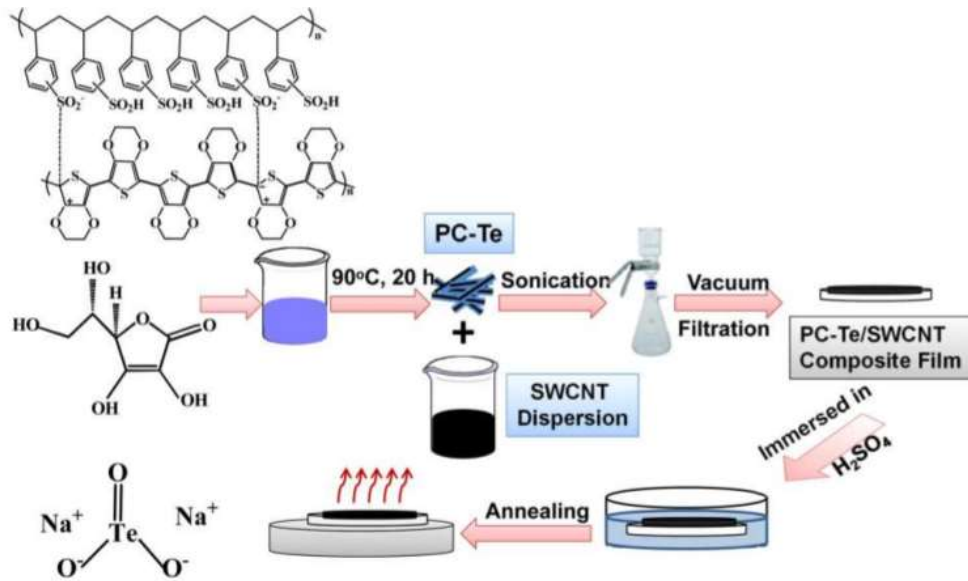
Fig. 17. Schematic illustration of the fabrication and post-treatment of the flexible SWCNT/PC-Te composite films [105].

Hu et al. [107] employed vacuum filtering for mixing the high mobility PEDOT nanowires with Te nanowires. The results revealed that adding Te nanowires increased the Seebeck coefficient of the Te NWs/PEDOT NWs composite films. However, its content should be kept up to 30wt%, leading to the optimal PF of 28 μW/mK^2. The authors reported that this is because, higher amount of Te nanowires had a converse effect on the electrical conductivity.

Despite the positive effect of adding Te to the polymer based TE materials on the PF of the hybrid composites, the scarce source of Te rises high cost issue, which hinders the commercialization of these high-performance hybrids. To reduce the prevalent required Te content (70-90wt%) without deteriorating the TE properties of these hybrid composites, Wang et al. [108] incorporated multiwalled carbon nanotubes (MWCNTs) in the Te nanorod/polyaniline (PANI) mixture. The results revealed that at room temperature the optimal PF of Te- MWCNT/PANI film was 54.4 μW/mK^2 with 52%Te and 16% MWCNT concentration. In fact, this PF was almost twice that of binary Te/PANI film with the same Te content. Rather than Te, Du et al [109] used BiTe based alloys to prepare Bi-Te based alloy nanosheet /PEDOT:PSS composite film by vacuum method. The results showed that in all temperatures, there was a tradeoff relationship between BTBA NS, as a Bi-Te based alloy, content and PF of the composite film. This was dominantly because of the inverse effect of BTBA NS content on the electrical conductivity. Thus, the maximum PF of 53 μW/mK^2 was achieved with minimum BTBA NS concentration of 10 wt%.

37

Tin selenide (SnSe) is also one of the most effective thermoelectric filler at nearly room temperature because of its outstanding Seebeck coefficient (~520 µV/K) and low thermal conductivity (~0.6 W/m·K) at 300 K [126].Therefore, Ju et al. [110,126] prepared a hybrid TE composite through incorporating SnSe nanosheets into a conducting polymer PEDOT:PSS matrix. The results indicated that although the content of SnSe nanosheets enhanced the Seebeck coefficient of the composites, but it remarkably reduced the electrical conductivity. To make a balance between Seebeck coefficient and the electrical conductivity, an optimal weight percentage of SnSe nanosheets was 20%, resulting in the highest PF of 390 µW/mK^2 at the room temperature.

Li et al. [111] utilized MoSe$_2$ to   improve the TE performance of PEDOT:PSS. The experiments were conducted by manipulating the MoSe$_2$ content in a range between 0-70 wt%. The results showed that the MoSe$_2$/PEDOT:PSS composite films obtained the highest PF of 48.6 µW/mK^2 with 5wt% MoSe$_2$ content, which was 1.7 order of magnitude higher than that of pristine PEDOT:PSS. Precisely, increasing the amount of MoSe$_2$ deteriorated the electrical conductivity, but increased the Seebeck coefficient till the MoSe$_2$ content was increased upto 7wt%. Obviously, the electrical conductivity and the Seebeck coefficient inversely depend on the carrier concentration. To address the improvement of both the electrical conductivity and the Seebeck coefficient simultaneously, Wang et al. [112] used layer by layer strategy to incorporate PEDOT:PSS with MoS$_2$ (ce-MoS$_2$) nanosheets. The PEDOT:PSS and ce-MoS$_2$ were alternately spin coated on a glass substrate, as shown in Fig. 18. The authors illustrated that DMSO, which the ce-MoS$_2$ nanosheets were dispersed in, reduced the PSS chains and aggregated the PEDOT chains. This was beneficial for the electron transport property of the composite films. Furthermore, high Seebeck coefficient of the PEDOT:PSS/ce-MoS$_2$ film was attributed to the energy filtering effect. To put it another way, the energy filtering process led the high energy carriers to transport, while hinders the low energy charge carriers, resulting in an enhanced Seebeck coefficient. The authors concluded that the PEDOT:PSS/ce-MoS$_2$ film achieved the highest PF of 41.6 µW/mK^2 with 4 number of layers. This amount was 5 order of magnitude higher than that of a single layer PEDOT:PSS film.
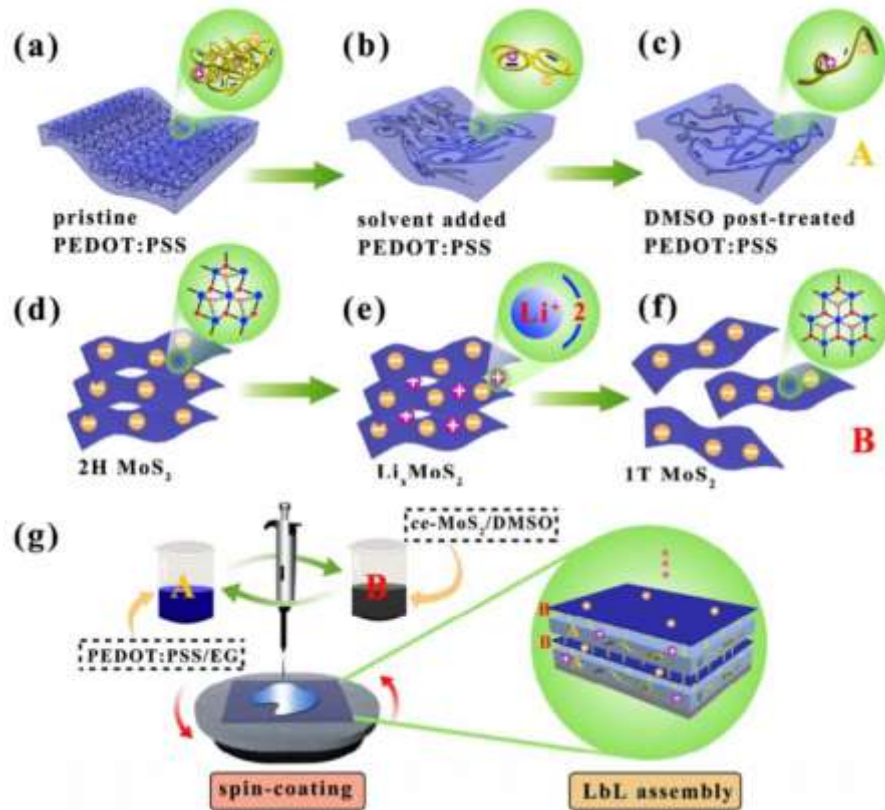
Fig. 18. The conformation evolution of PEDOT:PSS caused by chemical treatment (a) pristine PEDOT:PSS, (b) solvent added PEDOT:PSS, and (c) DMSO post-treated PEDOT:PSS; The exfoliation process of MoS2 (d) 2H phase MoS2, (e) LixMoS2, and (f) 1T phase MoS2; (g) The sketch of the spin-coating setup and the diagram of the PEDOT:PSS/ce-MoS2 heterostructure TE films [112].

The effect of nanostructuring on the TE properties of composite polymer films consisting of PEDOT:PSS and silicon nanoparticles (Si-NPs) has been studied by Saxena et al. [113] .The authors varied the Si-NPs content in the PEDOT:PSS/ Si-NP composite films in a range of between 0.3, 0.5, and 0.7 wt%. Adding 0.5 wt% Si-NPs to the pristine PEDOT:PSS, improved the power factor from 16.5 $\mu W/mK^2$ to 27.5 $\mu W/mK^2$. This improvement was related to the electrical conductivity reduction and enhancement of the Seebeck coefficient. The authors assigned this reduction to increasing of the Si-NPs content in the intermediate domains, resulting in percolation loss between different domains.

Apart from the conducting polymers, there are also other types of organic TE materials that can be used for hybrid TE composites. For example, Zheng et al. [114] proposed a new idea of multilayer composite structure with Sb_2Te_3 and CH3NH3I as an inorganic and organic TE materials, respectively. To prepare the layers, the CH3NH3I layer was encapsulated between two Sb_2Te_3 layers using thermal evaporation method. The CH3NH3I layer improved the electrical conductivity of the composite film due to promoting the growth of organic molecules

39

and the crystallization. Furthermore, post-annealing of the fabricated films enhanced the phonon scattering and ultimately reduced the thermal conductivity. The authors concluded that 1600 μW/mK^2 was the highest obtained PF of the composite at room temperature.

Li et al. [115] investigated a TE hybrid nanocomposite consisted of $Bi_{0.4}Sb_{1.6}Te_3$ alloy and graphene nanosheets (GNs). This incorporation resulted in higher carrier concentration, which improved the electrical conductivity of $Bi_{0.4}Sb_{1.6}Te_3$. Simultaneously, embedded graphene nanosheets reduced the lattice thermal conductivity of $Bi_{0.4}Sb_{1.6}Te_3$. This is because of the enhanced phonon scattering and the phase boundaries. The authors explained that at 300K, the highest PF of 4600 μW/mK^2 was recorded for 0.3 vol.% graphene nanosheets /$Bi_{0.4}Sb_{1.6}Te_3$ composite films. Zhang et al. [116] used carbon nanotubes (CNTs) for further improvement of $Bi_{0.4}Sb_{1.6}Te_3$ efficiency. Accordingly, the 0.1 wt% CNTs and $Bi_{0.4}Sb_{1.6}Te_3$ alloys were synthesized for 25 minutes under three different high pressures and high temperatures, including 2 GPa - 890 K, 3 GPa-910 K, and 4 GPa-930 K. The results showed that the synthesized sample under 2Gpa pressure was dominant concerning the power factor compared with the other two samples. As a result, at room temperature, $Bi_{0.4}Sb_{1.6}Te_3$ with 0.1 wt.% CNTs achieved the maximum PF of 3200 μW/mK^2 under 4Gpa synthesizing pressure. The authors assigned this high PF to the enhanced Seebeck coefficient associated to the lower energy carrier filtering.

Since the insertion of CNTs improves simultaneously improves the electrical transport properties and phonon scattering, Lei et al. [118] introduced multi-walled carbon nanotube (MWCNTs) into an MgAgSb based TE material to improve its TE performance. The results showed that the CNT coated $MgAg_{0.97}Sb_{0.99}$ facilitated electrical transport and phonon scattering. Therefore, the electrical conductivity increased sharply by increasing the CNTs content from 0.1wt% to 0.75wt%. However, the Seebeck coefficient was directly related to the effective mass (m*) of the compound, where the m* of the compound decreased by increasing the MWCNT content up to 0.2wt%, but then relatively increased. The authors explained that increasing the CNT content increases the MgAgSb/CNTs interfaces, resulting in lower thermal conductivity. The work indicated 0.1wt% as the optimal CNT content at room temperature, which resulted in almost 20% greater PF compared with CNT free $MgAg_{0.97}Sb_{0.99}$.

The interdependent nature of Seebeck coefficient and electrical conductivity should be overcome to achieve higher Seebeck coefficient without compromising the electrical conductivity. Accordingly, the inorganic particles should strongly and uniformly attach the polymer chains. To enhance this interaction and reduce the contact resistance, the inorganic

particle could be defects induced. Goo et al. [117] improved the interaction between PEDOT:PSS and Bi_2Te_3 in Bi_2Te_3/PEDOT:PSS composite thin films through the creation of additional defects in Bi_2Te_3 via proton irradiation. The results showed that the irradiation formed Bi-rich Bi_2Te_3 and Bi_{Te} antisite defects. The authors reported that both the Seebeck coefficient and the electrical conductivity enhanced with an increase in the proton energy, leading to the optimal PF of 432 $\mu W/mK^2$.

5.2. N type hybrid TE materials

The high electrical conductivity of inorganic TE materials and low thermal conductivity of organic TE materials provide immense potentials for inorganic–organic TE materials to obtain high PF. Furthermore, air stability is a crucial factor for n type organic TE materials to prevent them to return into positive Seebeck coefficient after exposure to air over a period of time. Nonoguchi et al. [119] tried to enhance air stability of an n type SWCNT by treating it with a series of ordinary salts and crown ethers. The studied salts included sodium chloride (NaCl), sodium hydroxide (NaOH), and potassium hydroxide (KOH)). The results revealed that dipping SWCNT into the stock solution of 0.1 mol/L KOH and 18-crown--ether resulted in an n type composite film with the highest PF of 230 $\mu W/mK^2$, which its air stability was for more than one month. Zaia et al. [120] coated Te nanowires with PDI as an air stabile organic component to achieve PDI-Te composite, as shown in Fig. 19. Different volume ratios of PDI was considered for synthesizing. However, the highest PF of 17.6 $\mu W/mK^2$ was achieved by 80 vol% PDI concentration.
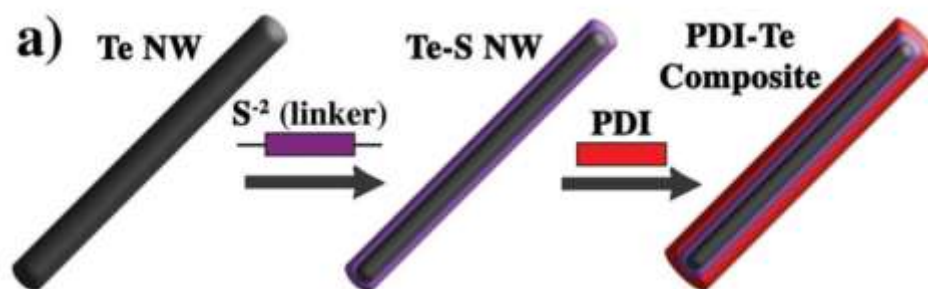
Fig. 19. Cartoon depiction of platform-based design scheme for n-type hybrid nanostructures [120].

A simple scale-up fabrication protocols was proposed by Chen et al. [121], who embedded Nickel (Ni) nanowires within PVDF matrix without the need for a doping treatment. The

authors prepared the n type Ni/PVDF films by mixing the Ni nanowires with PVDF powder in dimethylformamide (DMF) solution. The results revealed that increasing the Ni nanowire content from 20-80wt% increased the carrier mobility, and leading to higher electrical conductivity. However, an increase in the Ni nanowire content had no effect on the Seebeck coefficient. The study concluded that the n type Ni/PVDF films obtained the notably high PF of 200 μW/mK^2 with 80 wt% Ni nanowires. Luo et al. [122] converted the composite of polypropylene (PP), as an insulating polymer , CNTs , and CuO into an n type TE material by adding polyethylene glycol (PEG). The results revealed that although adding 8 wt% PEG switched the p type composite into an n type, but the prepared PP-CNT-CuO-PEG composite obtained the highest power factor of 0.78 μW/mK^2 with 2wt% CNT, 5 wt% CuO and 10 wt% PEG concentration.

Wu et al. [123] took advantage of high electrical conductivity of a SWCNT and the large Seebeck coefficient of perylene diimide (PDINE) and naphthalene diimide (NDINE) to yield n type hybrid TE composites. The experiments were conducted by mixing SWCNT by either PDINE or NDINE. The obtained PDINE/SWCNT and NDINE/SWCNT composites displayed greatly enhanced power factors of 112 $\pm$ 8 μW/mK^2 and 135 $\pm$ 14 μW/mK^2, respectively. Gao et al. [124], used a series of terminal tertiary amine groups of ADTA (a-g) to yield n type SWCNT/ADTA composite films. The result showed that the number of side chains and type of the terminal amine greatly affected the electrical conductivity and the Seebeck coefficient of the prepared composite films. In particular, the SWCNT/ADTAb composite films displayed the highest PF value of 124.4 $\pm$ 10.5 μW/mK^2 at room temperature.

Since the power factors of all these n-type polymer composites are still low compared with state-of-the-art inorganic thermoelectric semiconductors, there is an emerging direction to make a hybrid inorganic/organic superlattice. Wan et al. [125] used superlattice method to incorporate TBA and TA molecules as two kinds of organic TE materials with TiS$_2$ to yield n type TiS$_2$(TBA)$_{0.013}$(HA)$_{0.019}$, as shown in Fig. 20. The lower carrier concentration of TiS$_2$(TBA)$_{0.013}$(HA)$_{0.019}$ compared to that of pure TiS$_2$ crystalline resulted in higher electrical conductivity and lower thermal conductivity. The authors recorded the highest PF of 904 μW/mK^2 for TiS$_2$(TBA)$_{0.013}$(HA)$_{0.019}$ thin films at 300K.
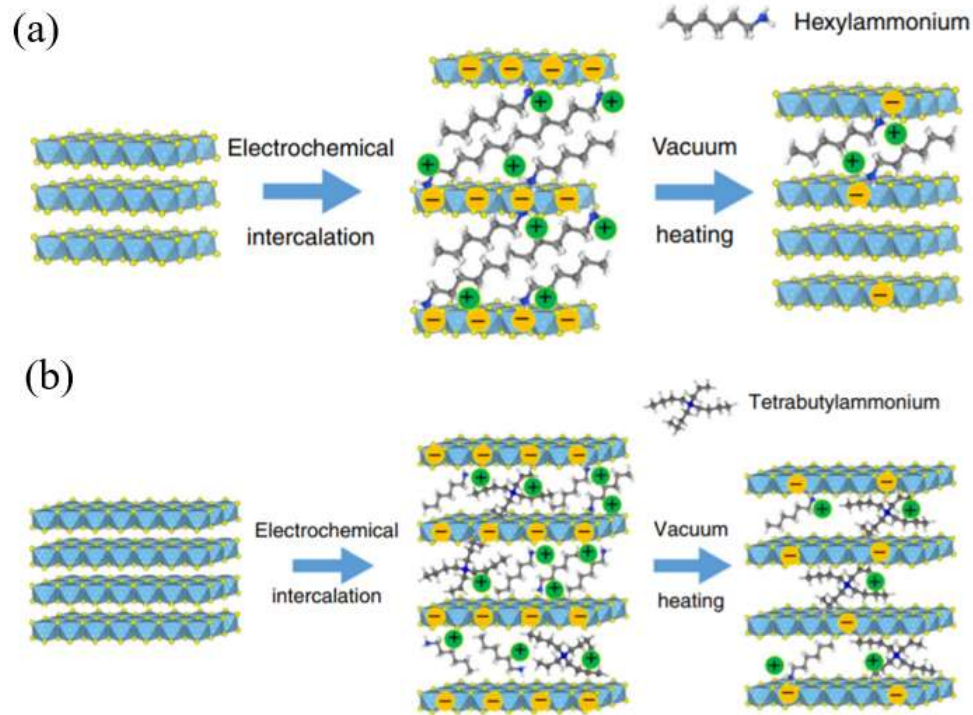
Fig. 20. a) Evolution of structure and carrier concentration of TiS2 single crystal with the electrochemical intercalation of HA molecules and vacuum heating, b) Evolution of structure and carrier concentration of TiS2 single crystal with the electrochemical intercalation of HA/TBA molecules and vacuum heating [125].

6. Flexible wearable TEGs

The main focus of sections 3 to 5 has been on the recently developed TE materials and their efficiencies at room temperature. This is essential because the effective temperature difference which can be utilized from body heat is small. Therefore, one strategy is optimizing the efficiency of the TE materials employed in the wearable TEGs. However, another typical requirement for wearable TEGs is to be flexible, and as such a major emerging trend is the development of flexible wearable TEGs. Accordingly, the most common approaches are either to deposit thin legs of inorganic material on a flexible substrate or to use fully organic or hybrid TE materials, because thery are intrinsically flexible.

6.1. Flexible TEGs with inorganic TE materials

Among various methods to generate flexible TEGs, wet deposition of thermoelectric thick films onto flexible substrates such as plastics and textiles is the most promising one. In general, wet deposition of the thermoelectric materials can be conducted using different techniques, such as sputtering, dispenser printing, inject printing and screen printing. Cao et al. [127] used screen printing technique to fabricate a polyimide substrate with $Bi_{1.8}Te_{3.2}$ (as n legs) and

43

Sb_2Te_3 (as p legs) pastes. The experiment was conducted in five steps. First, a stencil was placed on the substrate as a mask. Second, the thermoelectric pastes were added to the stencil and spread over the substrate by a blade. Then, a pressure squeegee passed across the stencil to force the pastes through its openings onto the substrate. Next, the stencil was lifted off from the substrate to leave the patterned thermoelectric pastes on the substrate. Finally, the experiment was finished by drying the pasted substrate at 353K for 2 minutes and curing it at 523 K for 3 hours in a N_2 atmosphere. The results showed that using SbTe as electrodes, the prepared flexible TEG obtained the highest power output of 16.34 nW/cm^2 at 293K temperature difference, which resembles the average temperature difference between human body and ambient in cold months.

Varghese et al. [128] developed an ink based $Bi_2Te_{2.8}Se_{0.2}$ to be screen printed on flexible polyimide substrates. The authors prepared the nanocrystals of $Bi_2Te_{2.8}Se_{0.2}$ using a microwave –stimulated wet-chemical method. Then, the ink was screen printed on flexible polyimide substrates using a screen mesh. Next, the printed films were dried on a hot plate at 473K to remove the used solvent and binders, followed by a cold compaction to consolidate the films. Finally, the films were sintered at 703K for 45 minutes in vacuum. While thin copper foils were applied as electrodes, the authors reported that 0.5mW/cm^2 was the greatest achieved power output at a temperature difference of 293K.

Chen et al [129] generated a highly flexible inject printed TEG using Bi_2Te_3 and $Bi_{0.5}Sb_{1.5}Te_3$ nanowires as n and p type legs respectively. The authors demonstrated that the prepared TE inks were inject printed on a polyimide substrate. After that, the printed TE films were annealed in a tube furnace under forming gas to improve their TE properties. It is notable that the TE legs were connected to each other using EGaIn liquid metal. The experiment was finished by coating the final device with a silicon elastomer to protect it from the environment. The results showed that the printed TEG delivered a maximum power output of 127nW, when the temperature difference was 32.5K.

6.2. *Flexible TEGs with organic TE materials*

Printing of thin-film thermoelectric devices is also applicable for organic TE materials. Zhang et al. [130] employed a roll to roll system to fabricate a rectangular flexible TEG with Nitrogen-

doped graphene inks as n-type legs and PEDOT: PSS inks both as p-type legs and electrodes. The inks were printed on the flexible plastic substrate with tunable rotation pressure and speed. Then, the printed plastic substrate was treated by UV irradiation in open air for one hour. Subsequently, it was subjected to oxygen plasma treatment for an hour. The authors illustrated a maximum power output of ~0.024μW/cm^2 at ΔT=283K. Stepien et al. [131] dispenser printed 61 unipolar p type legs made up of PEDOT: PSS on a glass substrate, and connected them with silver paste as a form of electrode. The results showed that at a temperature gradient of 90K, the maximum recorded power output was ~100nW. Liu et al. [132] electrochemically injected n type poly[Kx(Ni-ethylenetetrathiolate)] film on a polyethylene terephthalate (PET) substrate. The n type films patterned on the substrate by a PDMS mask. Then the TE legs were connected in series with gold conjunctions. The results indicated that at a temperature gradient of 12 K, the best power density reached up to 577.8 μW/cm^2.

Instead of film shape TEGs, Wu & Hu [133] introduced a fiber shape TEG by coating commercial polyester yarns with organic composites, resulting in the p type and n type legs. Accordingly, the authors used NWPU/PEDOT: PSS/multi-walled carbon nanotube (MWCNT) and NWPU/nitrogen doped multi-walled carbon nanotube (N-MWCNT) as the p-type and n-type thermoelectric composites, respectively. Then, the prepared p-type and n-type yarns were embroidered into the lock-nit surface of a spacer fabric and arranged alternatively. Finally, every adjacent p-type and n-type yarns were connected using silver paint at the top and bottom of the yarns' loops. The results exhibited that the 3D fabric TEG ,comprised of 10 thermocouples, produced the maximum power of 0.21 nW/cm^2 at ΔT= 66 K. More recently, Ito et al. [134] prepared an integrated p/n stripe patterned CNT thread by doping a p-type CNT_PEG composite thread with 1-butyl-3-methylimidazolium hexafluorophosphate ([BMIM]PF6) as an n type doping agent. Then, the stripe patterned thread was sewn into a piece of fabric with 3 mm thick and 4cm^2 base area. The authors concluded that a maximum power output of 0.125 nW/cm^2 was generated by the prototype owing to the body heat.

6.3. *Flexible TEGs with hybrid TE materials*

Jung et al. [135] aimed to generate a flexible TE module by distributing a hybrid TE material within highly flexible polydimethyl siloxane (PDMS). To reach the aim, the authors seperately mixed Bi (p-type) and Te (n-type) with carbon nanotubes (CNTs) to improve their electrical conductivities. Consequently, the hybrid TE powders were added to a solution of PDMS as a

precursor. Then the composites were poured into the holes of a pored aluminum plate, followed by curing for 3 hours at 363K to make the pillar shape thermoelectric legs. The authors demonstrated that the pillar structures of the thermoelectric legs were sandwiched between extra PDMS to enhance their flexibility, and then connected to each other with aluminum electrodes. The results showed that the prepared flexible TEG generated the greatest power output of 80μW / cm^2 at ΔT=293K.

Bae et al. [136] prepared a flexible TEG using Te-PEDOT: PSS hybrid composite. The experiment was started by optimizing the electrical conductivity of the Te-PEDOT: PSS composite by simple chemical treatment with H_2SO_4 . Consequently, the H_2SO_4 treated Te-PEDOT: PSS solutions were deposited on a flexible glass substrate as p type thermoelectric legs, followed by connecting to each other with silver electrodes. The results showed that a maximum power output of 0.7 nW/cm^2 was delivered from a 15 cm^2 TEG area in response to heat from human body. In another work, rather than chemical treatment, Bae et al. [137] used two additives individually to enhance the electrical conductivity of the Te-PEDOT: PSS hybrid composite. The additives were graphene nanoparticles (GNPs) and single-walled CNTs (SSWNTs). Then the two samples were sprayed separately on a glass substrate through a spray printing technique. The results showed that the two flexible TEGs generated a maximum power output of 1.7 nW/cm^2 and 31.5 nW/cm^2 with 8 wt% GNPs and 3wt% SSWNTs contents, respectively.

7.   Conclusions and outlook

Out of various strategies to improve the efficiency of inorganic TE materials, the most promising ones are increasing hole concentration and phonon scattering, besides decreasing lattice thermal conductivity. To put it another way, employing these strategies increases the $Z\overline{T}$ values of inorganic TE materials up to a range between 1.15 and 1.36. In particular, only $Bi_{0.4-x}Sb_{1.6+x}Te_3$, which is a p type alloy, is able to reach this maximum $Z\overline{T}$ range. Regarding n type inorganic TE materials, in general , maximum $Z\overline{T}$ values are achieved by $Bi_2Te_{2.7}Se_{0.3}$ in a range between 0.7 and 0.8, which is lower than that of the p type counterpart. In respect of inorganic TE materials fabrication, hot pressing is superior compared with spark plasma sintering, ball milling, and zone melting. It can be seen from the review that among the two types of organic TE materials, the power factors of carbon based TE composites are dominant

compared with those of the polymer based counterparts. Furthermore, the greatest power factor for p type carbon based TE composites is achieved by layer by layering deposition process. Whereas for n type carbon based composites, the most striking approach is combination of n type dopants and annealing treatment. Like organic TE materials, hybrid TE materials containing a carbon based TE material show higher power factor than those composed of polymer based TE materials. To illustrate, combination of graphene or carbon with $Bi_{0.4}Sb_{1.6}Te_3$ leads to the most striking hybrid TE materials.

It can be seen from the review that although inorganic TE materials benefit from almost high ZT value (~1), but they suffer from rigidity, rarity in the earth's crust, and containing toxic elements. Conversely, organic TE materials benefit from higher flexibility and absence of toxic elements. However, there are two main problems with organic TE materials. First, they are mostly p type and their n type is still lacking attributed to the poor stability of n type conducting polymers in air. Second, optimizing the PF of organic TE materials depends on effective methods, including doping, de doping, post treatment, crystallinity, or alignment, while these technological process and conditions required to be optimized. Therefore, hybrid TE materials have attracted the most attention in recent years. This is because they can be a promise to solve the rigidity of inorganic TE materials and low efficiency of the organic counterparts, which are desirable for wearable TEGs. However, hybrid TE materials still suffer from containing toxic and rare inorganic elements, lower efficiency relative to the inorganic TE materials, and air instability of their n type. In addition, until to date, TE materials are only examined with respect to their efficiency and no research is carried out on their lifecycle performance aspect. Therefore, as part of the sustainability criteria for future technologies, the environmental performance of any energy technology requires careful attention. This part is heavily neglected in the existing research on TE materials, which should be addressed in future.

References

[1]   IEA. Electricity Statistics Detailed, comprehensive annual data on electricity and heat, Available at: https://www.iea.org/statistics/electricity; [Accessed May 05 2019].

[2]   IEA. Statistics Global energy data at your fingertips, Available at: https://www.iea.org//statistics/?country=WORLD&year=2016&category=Electricity&indicator=ElecGenByFuel&mode=chart&dataTable=ELECTRICITYANDHEAT; [Accessed May 05 2019].

[3]   Wang L, Zhang Z, Liu Y, Wang B, Fang L, Qiu J, Zhang K, Wang S. Exceptional thermoelectric properties of flexible organic-inorganic hybrids with monodispersed and periodic nanophase. Nat Commun 2018;9(1). https://doi.org/10.1038/s41467-018-06251-9.

[4]   IEA. Renewables, Available at: https://www.iea.org/topics/renewables; [Accessed May 05 2019].

[5]   Ren P, Liu Y, He J, Lv T, Gao J, Xu G. Recent advances in inorganic material thermoelectrics. Inorg Chem Front 2018;5:2380-2398. https://doi.org/10.1039/C8QI00366A.

[6]   Wang X, Liu Z, Zhang T. Flexible Sensing Electronics for Wearable/Attachable Health Monitoring. Small 2017;25(13):1602790. https://doi.org/10.1002/smll.201602790.

[7]   Nour Eddine A, Chalet, D, Faure X, Aixala L, Chessé P. Optimization and characterization of a thermoelectric generator prototype for marine engine application. Energy, 2018;143(682):695. https://doi.org/10.1016/j.energy.2017.11.018.

[8]   Siddique ARM, Mahmud S, Heyst BV. A review of the state of the science on wearable thermoelectric powergenerators (TEGs) and their existing challenges. Renewable Sustainable Energy Rev 2017;73:730-744. https://doi.org/10.1016/j.rser.2017.01.177.

[9]   Twaha S, Zhu J, Yan Y, Li B. A comprehensive review of thermoelectric technology: materials, applications, modelling and performance improvement. Renewable Sustainable Energy Rev 2016;65:698-726. https://doi.org/10.1016/j.rser.2016.07.034.

[10]   Champier D. Thermoelectric generators: A review of applications. Energy Convers Manage 2017;140:167-181. https://doi.org/10.1016/j.enconman.2017.02.070.

[11]   Kroon R, Mengistie DA, Kiefer D. Hynynen J, Ryan JD, Yua L, Müller C. Thermoelectric plastics: From design to synthesis, processing and structure–property relationships. Chem Soc Rev 2016;45:6147-6164. https://doi.org/10.1039/C6CS00149A.

[12]   Sajid M, Hassan I, Rahman A. An overview of cooling of thermoelectric devices. Renewable Sustainable Energy Rev 2017;78:15-22. https://doi.org/10.1016/j.rser.2017.04.098.

[13]   Du Y, Xu J, Paul B, Eklund P. Flexible thermoelectric materials and devices. Appl Mater Today 2018;12:366-388. https://doi.org/10.1016/j.apmt.2018.07.004.

[14]   Jin H, Li J, Iocozzia J, Zeng X, Wei P, Yang C, Li N, Liu Z, He JH, Zhu T, Wang J, Lin Z, Wang S. Hybrid organic-inorganic thermoelectric materials and devices. Angew Chem Int Ed 2019. https://doi.org/10.1002/anie.201901106.

[15]   Petsagkourakis I, Tybrandt K, Crispin X, Ohkubo I, Satoh N, Mori T. Thermoelectric materials and applications for energy harvesting power generation. Sci Technol Adv Mater 2018;19(1):836-862. https://doi.org/10.1080/14686996.

[16]   An CJ, Kang YH, Lee A, Jang K, Jeong Y, Cho SY. Foldable thermoelectric Materials: improvement of the thermoelectric performance of directly spun CNT webs by individual control of electrical and thermal conductivity. ACS Appl Mater Interfaces 2016;8(34). https://doi.org/10.1021/acsami.6b04485.

[17]   Li C, Jiang F, Liu C, Liu P, Xu J. Present and future thermoelectric materials toward wearable energy harvesting. Appl Mater Today 2019;15:543-557. https://doi.org/10.1016/j.apmt.2019.04.007.

[18]   Zhang Y, Heo YJ, Park M, Park SJ. Recent advances in organic thermoelectric materials: principle mechanisms and emerging carbon-based green energy materials. Polym 2019; 11(1):167. https://doi.org/10.3390/polym11010167.

[19]   Culebras M, Choi K, Cho C. Recent progress in flexible organic thermoelectrics. micromachines (Basel) 2018;9(12):30. https://doi.org/10.3390/mi9120638.

[20]   Yao H, Fan Z, Cheng H, Guan X, Wang C, Sun K, Ouyang J. Recent developments of thermoelectric polymers and composites. Macromol Rapid Commun 2018;39(6):1700727. https://doi.org/10.1002/marc.201700727.

[21]   Yao CJ, Zhang HL, Zhang Q. Recent progress in thermoelectric materials based on conjugated polymers. polym 2019;11(1):107. https://doi.org/10.3390/polym11010107.

[22] He R, Schierning G, Nielsch K. Thermoelectric devices: A review of devices, architectures, and contact optimization. Adv Mater Technol 2017;3(4):1700256. https://doi.org/10.3390/polym11010107.

[23] Shi X, Chen L, Uher C. Recent advances in high-performance bulk thermoelectric materials. Int Mater Rev 2016;61(6):379-415. https://doi.org/10.1080/09506608.2016.1183075.

[24] Chen X, Dai W, Wu T, Luo W, Yang J, Jiang W, Wang L. Thin film thermoelectric materials: Classification, characterization, and potential for wearable applications. Coat, 2018;8(7):244. https://doi.org/10.3390/coatings8070244.

[25] Jiang Q, Yang J, Liu Y, He H. Microstructure tailoring in nanostructured thermoelectric materials. J Adv Dielectr 2016;6(1):1630002. https://doi.org/10.1016/j.pnsc.2012.11.011.

[26] Chiu WT, Chen CL, Chen YY. A strategy to optimize the thermoelectric performance in a spark plasma sintering process. Sci Rep 2016;6:23143. https://doi.org/10.1038/srep23143.

[27] Mamur H, Bhuiyan MRA, Korkmaz F, Nil M. A review on bismuth telluride (Bi_2Te_3) nanostructure for thermoelectric applications. Renewable Sustainable Energy Rev 2018;82:4159-4169. https://doi.org/10.1016/j.rser.2017.10.112.

[28] Liu Z, Wang Y, Mao J, Geng H, Shuai J, Wang Y, He R, Cai W, Sui J, Ren Z. Lithium doping to enhance thermoelectric performance of MgAgSb with weak electron–phonon coupling. Adv. Energy Mater 2016; 6:1502269. https://doi.org/10.1002/aenm.201502269.

[29] Zheng Y, Liu C, Miao L, Lin H, Gao J, Wang X, Chen J, Wu S, Li X, Cai H. Cost effective synthesis of p-type Zn-doped MgAgSb by planetary ball-milling with enhancedthermoelectric properties. RSC Adv 2018;8:35353–35359. https://doi.org/10.1039/C8RA06765A.

[30] Liu Z, Mao J, Sui J, Ren Z. High thermoelectric performance of α-MgAgSb for power generation. Energy & Environmental Science 2018;11:23-44. https://doi.org/10.1039/c7ee02504a.

[31] Gao W, Yic X, Cui B, Wang Z, Huang J, Sui J, Liu Z. The critical role of Boron doping in the thermoelectric and mechanical properties of nanostructured α-MgAgSb. Journal of Materials Chemistry C 2018; 6: 9821-9827. https://doi.org/10.1039/C8TC03646B.

[32] Duan S, Man Na, Xu J, Wu Q, Liu GQ, Tan X, Shao H, Guo K, Yang X, Jiang J. Thermoelectric$(Bi,Sb)_2Te_3$-$Ge_{0.5}Mn_{0.5}Te$ composites with excellent mechanical properties. J Mater Chem A 2019;15:9241-9246. https://doi.org/10.1039/C9TA01962F.

[33] Wang YS, Huang LL, Li D, Zhang J, Qin XY. Enhanced thermoelectric performance of $Bi_{0.4}Sb_{1.6}Te_3$ based composites with CuInTe2 inclusions. J Alloys Compd 2018;758:72-77. https://doi.org/10.1016/j.jallcom.2018.05.035.

[34] Wang YS, Huang LL, Zhu C, Zhang J, Li D, Xin HX, Danish MH, Qin XY. Simultaneously enhanced power factor and phonon scattering in Bi0.4Sb1.6Te3 alloy doped with germanium. Scr Mater, 2018;154:118-122. https://doi.org/10.1016/j.scriptamat.2018.05.026.

[35] Hao F, Qiu P, Song Q, Chen H, Lu P, Ren D, Shi X, Chen L. Roles of Cu in the enhanced thermoelectric properties in $Bi_{0.5}Sb_{1.5}Te_3$. Mater (Basel), 2017;10(3):251. https://doi.org/10.3390/ma10030251.

[36] Guo X, Qin J, Jia X, Ma H, Jia H. Quaternary thermoelectric materials: Synthesis, microstructure andthermoelectric properties of the $(Bi,Sb)_2(Te,Se)_3$ alloys. J Alloys Compd 2017;705:363-368. https://doi.org/10.1016/j.jallcom.2017.02.182.

[37] Serrano-Sánchez F, Gharsallah M, Nemes NM, Biskup N, Varela M, Martínez JL, Fernández-Díaz MT, Alonso JA. Enhanced figure of merit in nanostructured $(Bi,Sb)_2Te_3$ with optimized composition, prepared by a straightforward arc-melting procedure. Sci Rep 2017;7:6277. https://doi.org/10.1038/s41598-017-05428-4.

[38] Liang S, Xu J, Wang H, Tan X, Liu GQ, Shao H, Yu B, Yue S, Jiang J. Investigation on structure and thermoelectric properties in p-type $Bi_{0.48}Sb_{1.52}Te_3$ via PbTe incorporating. J Mater Sci-Mater Electron 2018;29(9):7701-7706. https://doi.org/10.1007/s10854-018-8765-1.

49

[39] Gao N, Zhu B, Wang XY, Yu Y, Zu FQ. Simultaneous optimization of Seebeck, electrical and thermal conductivity in free-solidified $Bi_{0.4}Sb_{1.6}Te_3$ alloy via liquid-state manipulation. J Mater Sci 2018;53(12):9107-9116. https://doi.org/10.1007/s10853-018-2209-4.

[40] Fan Z, Wang H, Wu Y, Liu XJ, Lu ZP. Thermoelectric high-entropy alloys with low lattice thermal conductivity. RSC Adv 2016;6:52164-52170. https://doi.org/10.1039/C5RA28088E.

[41] Bochentyn B, Miruszewski T, Karczewski J, Kusz B. Thermoelectric properties of bismuth-antimony-telluride alloys obtained by reduction of oxide reagents. Mater Chem Phys 2016;177:353-359. https://doi.org/10.1016/j.matchemphys.2016.04.039.

[42] Liu Z, Zhang Y, Mao J, Gao W, Wang Y, Shuai J, Cai W, Sui J, Ren Z. The microscopic origin of low thermal conductivity for enhanced thermoelectric performance of Yb doped MgAgSb. Acta Materialia 2017; 128: 227-234. https://doi.org/10.1016/j.actamat.2017.02.015.

[43] Lei J, Zhang D, Guan W, Cheng Z, Wang C, Wang Y. Engineering Electrical Transport in α-MgAgSb to Realize High Performances near Room Temperature. Physical Chemistry Chemical Physics 2018; 20: 16729-16735. https://doi.org/10.1039/C8CP02186D.

[44] Liu Z, Shuai J, Mao J, Wang Y, Wang Z, Cai W, Sui J, Ren Z. Effects of antimony content in MgAg0.97Sbx on output power and energy conversion efficiency. Acta Materialia 2016; 102:17-23. https://doi.org/10.1016/j.actamat.2015.09.033.

[45] Liu Z, Wang Y, Gao W, Mao J, Geng H, Shuai J, Cai W, Sui J, Ren Z. The influence of doping sites on achieving higher thermoelectric performance for nanostructured α-MgAgSb. Nano Energy 2017; 31: 194-200. https://doi.org/10.1016/j.nanoen.2016.11.010.

[46] Zheng Y, Liu C, Miao L, Li C, Huang R, Gao J, Wang X, Chen J, Zhou Y, Nishibori E. Extraordinary thermoelectric performance in MgAgSb alloy with ultralow thermal conductivity. Nano Energy 2019; 59;311-320. https://doi.org/10.1016/j.nanoen.2019.02.045.

[47] Deng R, Su X, Zheng Z, Liu W, Yan Y, Zhang Q, P. Dravid V, Uher C, G. Kanatzidis M, Tang X. Thermal conductivity in Bi0.5Sb1.5Te3+x and the role of dense dislocation arrays at grain boundaries. Sci Adv 2018; 4(6): 5606. https://doi.org/10.1126/sciadv.aar5606.

[48] Hao F, Xing T, Qiu P, Hu P, Wei T, Ren D, Shi X, Chen L. Enhanced thermoelectric performance in n-type Bi_2Te_3- based alloys via suppressing intrinsic excitation. ACS Appl Mater Interfaces 2018;10(25):21372-21380. https://doi.org/10.1021/acsami.8b06533.

[49] Kang Y, Zhang Q, Fan C, Hu W, Chen C, Zhang L, Yu F, Tian Y, Xu B. High pressure synthesis and thermoelectric properties of polycrystalline Bi_2Se_3. J Alloys Compd 2017;700:223-227. https://doi.org/10.1016/j.jallcom.2017.01.062.

[50] Nozariasbmarz A, Krasinski JS, Vashaee D. N-Type bismuth telluride nanocomposite materials optimization for thermoelectric generators in wearable applications. Mater, 2019;12(9):1529. https://doi.org/10.3390/ma12091529.

[51] Zhu B, Huang ZY, Wang XY, Yu Y, Gao N, Zu FQ. Enhanced thermoelectric properties of n-type direction solidified $Bi_2Te_{2.7}Se_{0.3}$ alloys by manipulating its liquid state. Scr Mater 2018;146:192-195. https://doi.org/10.1016/j.scriptamat.2017.11.045.

[52] Zhu B, Yu Y, Wang XY, Zu FQ, Huang ZY. Enhanced thermoelectric properties of n-type $Bi_2Te_{2.7}Se_{0.3}$ semiconductor by manipulating its parent liquid state. J Mater Sci 2017;52(14):8526-8537. https://doi.org/10.1007/s10853-017-1063-0.

[53] Wang X, Wang H, Xiang B, Shang H, Zhu B, Yu Y, Jin H, Zhao R, Huang Z, Liu L, Zu F, Chen Z. Attaining reduced lattice thermal conductivity and enhanced electrical conductivity in as-sintered pure n-type Bi_2Te_3 alloy. J Mater Sci 2019;(54)6:4788-4797. https://doi.org/10.1007/s10853-018-3172-9.

[54] Hong M, Chasapis TC, Chen Z, Yang L, Kanatzidis MG, Snyder GJ, Zou J. n-Type $Bi_2Te_{3-x}Se_x$ nanoplates with enhanced thermoelectric efficiency driven by wide frequency phonon scatterings and synergistic carrier scatterings. ACS Nano, 2016;10(4):4719-4727. https://doi.org/10.1021/acsnano.6b01156.

[55] Yang L, Chen Z, Dargusch MS, Zou J. High Performance Thermoelectric Materials: Progress and Their Applications. Adv Energy Mater 2017;8(6):1701797. https://doi.org/10.1002/aenm.201701797.

[56]   Hao F, Qiu P, Tang Y, Bai S, Xing T, Chu H, Zhang Q, Lu P, Zhang T, Ren D, Chen J, Shi X, Chen L. High efficiency Bi2Te3-based materials and devices for thermoelectric power generation between 100 and 300 °C. Energy Environ Sci 2016;9:3120-3127. https://doi.org/10.1039/C6EE02017H.

[57]   Madavali B, Kim H, Lee K, Hong S. Enhanced Seebeck coefficient by energy filtering in Bi-Sb-Te based composites with dispersed Y_2O_3 nanoparticles. Intermetallics, 2017;82:68-75. https://doi.org/10.1016/j.intermet.2016.11.002.

[58]   Cao B, Jian J, Ge B, Li S, Wang H, Liu J, Zhao H. Improved thermoelectric performance in p-type Bi0.48Sb1.52Te3 bulk material by adding $MnSb_2Se_4$. Chin Phys 2017;26:017202. https://doi.org/10.1088/1674-1056/26/1/017202.

[59]   Kim SI, Lee KH, Mun HA, Kim HS, Hwang SW, Roh JW, Yang DJ, Shin WH, Li XS, Lee YH, Snyder GJ, Kim SW. Dense dislocation arrays embedded in grain boundaries for high-performance bulk thermoelectrics. Science 2015; 348(6230):109-114. https://doi.org/10.1126/science.aaa4166.

[60]   Jang H, Park YJ, Chen X, Das T, Kim M, Ahn J. Graphene-based flexible and stretchable electronics. Adv Mater 2016;28(22):4184-4202. https://doi.org/10.1002/adma.201504245.

[61]   Wang M, Baek P, Akbarinejad A, Barkerab D, Travas-Sejdic J. Conjugated polymers and composites for stretchable organic electronics. J Mater Chem C 2019;7(19), 5534-5552. https://doi.org/10.1039/C9TC00709A.

[62]   Bhosale ME, Chae S, Kim JM, Choi J. Organic small molecules and polymers as an electrode material for rechargeable lithium ion batteries. J Mater Chem A, 2018;6:19885-19911. https://doi.org/10.1039/C8TA04906H.

[63]   Kolasińska E, Kolasiński P. A review on electroactive polymers for waste heat recovery. mater (Basel) 2016;9(6). doi: https://doi.org/10.3390/ma9060485.

[64]   Ni D, Chen Y, Song H, Liu C, Yanga X, Cai K. Free-standing and highly conductive PEDOT nanowire films for high-performance all-solid-state supercapacitors. J Mater Chem A, 2019;7:1323-1333. https://doi.org/10.1039/C8TA08814D.

[65]   Lu Y, Qiu Y, Cai K, Ding Y, Wang M, Jiang C, Yao Q, Huang C, Chen L, He J. Ultrahigh power factor and flexible silver selenide-based composite film for thermoelectric devices. Energy Environ Sci 2019. https://doi.org/10.1039/C9EE01609K.

[66]   Du Y, Cai KF, Shen SZ, Donelsonand R, Xu JY, Wang HX, Lin T. Multifold enhancement of the output power of flexible thermoelectric generators made from cotton fabrics coated with conducting polymer. RSC Adv 2017;7:43737-43742. https://doi.org/10.1039/C7RA08663F.

[67]   Fan Z, Li P, Du D, Ouyang J. Significantly Enhanced Thermoelectric Properties of PEDOT:PSS Films through Sequential Post-Treatments with Common Acids and Bases. Adv Energy Mater 2017;7(8):1602116. https://doi.org/10.1002/aenm.201602116.

[68]   Jung IH, Hong CT, Lee U, Kang YH, Jang K, Cho SY. High Thermoelectric Power Factor of a Diketopyrrolopyrrole-Based Low Bandgap Polymer via Finely Tuned Doping Engineering. Sci Rep 2017;7:44704. https://doi.org/10.1038/srep44704.

[69]   Zhang L, Goto T, Imae I, Sakurai Y, Harima Y, Thermoelectric Properties of PEDOT Films Prepared by Electrochemical Polymerization. J polym sci 2016;55(6):524-531. https://doi.org/10.1002/polb.24299.

[70]   Patel SN, Glaudell AM, Kiefer D, Chabinyc ML. Increasing the Thermoelectric Power Factor of a Semiconducting Polymer by Doping from the Vapor Phase. Macro Lett 2016;5(3):268-272. https://doi.org/10.1021/acsmacrolett.5b00887.

[71]   Lim E, Peterson KA, Su GM, Chabinyc ML. Thermoelectric properties of poly(3-hexylthiophene) (P3HT) doped with 2,3,5,6-Tetrafluoro-7,7,8,8-tetracyanoquinodimethane (F_4TCNQ) by vapor-phase infiltration. ChemMater 2018;30(3):998-1010. https://doi.org/10.1021/acs.chemmater.7b04849.

[72]   Li H, DeCoster ME, Ireland RM, Song J, Hopkins PE, Katz HE. Modification of the Poly(bisdodecylquaterthiophene) Structure for High and Predominantly Nonionic Conductivity

with Matched Dopants. J Am Chem Soc 2017;139(32):11149-11157. https://doi.org/10.1021/jacs.7b05300.

[73] Pan C, Wang L, Liu T, Zhou X, Wan T, Wang S, Chen Z, Gao C, Wang L. Polar Side Chain Effects on the Thermoelectric Properties of Benzo[1,2-b:4,5-b′]Dithiophene-Based Conjugated Polymers. Macromol Rapid Commun 2019;40(12):1900082. https://doi.org/10.1002/marc.201900082.

[74] Wang L, Pan C, Liang A, Zhou X, Zhou W, Wana T, Wang L. Effect of Backbone Structure on the Thermoelectric Properties of Donor-acceptor Conjugated Polymers. Polym Che 2017;8:4644-4650. https://doi.org/10.1039/C7PY01005B.

[75] Wang X, Kyaw AKK, Yin C, Wang F, Zhu Q, Tang T, Yee PI, Xu J. Enhancement of thermoelectric performance of PEDOT:PSS films by post-treatment with a superacid. RSC Adv 2018;8:18334-18340. https://doi.org/10.1039/C8RA02058B.

[76] Un H, Gregory SA, Mohapatra SK, Xiong M, Longhi E, Lu Y, Rigin S, Jhulki S, Yang C, Timofeeva TV, Wang J, Yee SK, Barlow S, Marder SR, Pei J. Understanding the Effects of Molecular Dopant on n-Type Organic Thermoelectric Properties. Adv Energy Mater 2019;9(24), 1900817. https://doi.org/10.1002/aenm.201900817.

[77] Gao F, Liu Y, Xiong Y, Wu P, Hu B, Xu L. Fabricate organic thermoelectric modules use modified PCBM and PEDOT:PSS materials. Front OptoElectron 2017;10(2):117-123. https://doi.org/10.1007/s12200-017-0712-x.

[78] Hwang S, Potscavage Jr. WJ, Yang YS, Park IS, Matsushima T, Adachi C. Solution-processed organic thermoelectric material exhibiting doping-concentration-dependent polarity. Phys Chem Chem Phys 2016;18:29199-29207. https://doi.org/10.1039/C6CP04572C.

[79] Huang D, Yao H, Cui Y, Zou Y, Zhang F, Wang C, Shen H, Jin W, Zhu J, Diao Y, Xu W, Di C, Zhu D. Conjugated-Backbone Effect of Organic Small Molecules for n Type Thermoelectric Materials with ZT over 0.2. J Am Chem Soc 2017;139(37):13013-13023. https://doi.org/10.1021/jacs.7b05344.

[80] Yang C, Jin W, Wang J, Ding Y, Nong S, Shi K, Lu Y, Dai Y, Zhuang F, Lei T, Di C, Zhu D, Wang J, Pei J. Enhancing the n-Type Conductivity and Thermoelectric Performance of Donor–Acceptor Copolymers through Donor Engineering. Adv mater 2018;30(43):1802850. https://doi.org/10.1002/adma.201802850.

[81] Tomlinson EP, Mukherjee S, Boudouris BW. Enhancing polymer thermoelectric performance using radical dopants. Org Electron 2017;51:243-248. https://doi.org/10.1016/j.orgel.2017.09.029.

[82] Madan D, Zhao X, Ireland RM, Xiao D, Katz HE. Conductivity and power factor enhancement of n-type semiconducting polymers using sodium silica gel dopant. APL Mater (Basel) 2017;5(8):086106. https://doi.org/10.1063/1.4990139.

[83] Punetha VD, Rana S, Yoo HJ, Chaurasia A, McLeskey Jr, JT, Ramasamy MS, Sahoo NG, Cho JW. Functionalization of carbon nanomaterials for advanced polymer nanocomposites: A comparison study between CNT and graphene. Prog Polym Sci 2017;67:1-47. https://doi.org/10.1016/j.progpolymsci.2016.12.010.

[84] Wang L, Yao Q, Xiao J, Zeng K, Qu S, Shi W, Wang Q, Chen L. Engineered Molecular Chain Ordering in Single-Walled Carbon Nanotubes/Polyaniline Composite Films for High-Performance Organic Thermoelectric Materials. Chem Asian J 2016;11(12):1804-1810. https://doi.org/10.1002/asia.201600212.

[85] Wang Y, Yang J, Wang L, Du K, Yin Q, Yin Q. Polypyrrole/Graphene/Polyaniline Ternary Nanocomposite with High Thermoelectric Power Factor. ACS Appl Mater Interfaces 2017;9(23):20124-20131. https://doi.org/10.1021/acsami.7b05357.

[86] Wang S, Liu F, Gao C, Wan T, Wang L, Wang L, Wang L. Enhancement of the thermoelectric property of nanostructured polyaniline/carbon nanotube composites by introducing pyrrole unit onto polyanilinebackbone via a sustainable method. Chem Eng J 2019;307, 322-329. https://doi.org/10.1016/j.cej.2019.03.155.

[87]   Lee W, Kang YH, Lee JY, Jang K, Cho SY. Improving the thermoelectric power factor of CNT/PEDOT:PSS nanocomposite films by ethylene glycol treatment. RSC Adv 2016;6:53339-53344. https://doi.org/10.1039/C6RA08599G.

[88]   Jiang Q, Lan X, Liu C, Shi H, Zhu Z, Zhao F, Xu J, Jiang F. High-performance hybrid organic thermoelectric SWNTs/PEDOT:PSS thin-films for energy harvesting. Mater Chem Front 2018;2:679-685. https://doi.org/10.1039/C7QM00515F.

[89]   Cho C, Wallace KL, Tzeng P, Hsu J, Yu C, Grunlan JC. Outstanding Low Temperature Thermoelectric Power Factor from Completely Organic Thin Films Enabled by Multidimensional Conjugated Nanomaterials. Adv Energy Mater 2016;6(7):1502168. https://doi.org/10.1002/aenm.201502168.

[90]   Park C, Yoo D, Lee JJ, Choi HH, Kim JH. Enhanced power factor of poly (3,4-ethyldioxythiophene):poly (styrene sulfonate) (PEDOT:PSS)/RTCVD graphene hybrid films. Org Electro 2016;36:166-170. https://doi.org/10.1016/j.orgel.2016.05.038.

[91]   Cho C, Culebras M, Wallace KL, Song Y, Holder K, Hsu J, Yu C, Grunlan JC. Stable n-type thermoelectric multilayer thin films with high power factor from carbonaceous nanofillers. Nano Energy 2016;28:426-432. https://doi.org/10.1016/j.nanoen.2016.08.063.

[92]   Zhou W, Fan Q, Zhang Q, Cai L, Li K, Gu X, Yang F, Zhang N, Wang Y, Liu H, Zhou W, Xie, S. High-performance and compact-designed flexible thermoelectric modules enabled by a reticulate carbon nanotube architecture. Nat Commun 2017;8:14886. https://doi.org/10.1038/ncomms14886

[93]   Horike S, Fukushima T, Saito T, Kuchimura T, Koshiba Y, Morimotoac M, Ishida K. Highly stable n-type thermoelectric materials fabricated via electron doping into inkjet-printed carbon nanotubes using oxygen-abundant simple polymers. Mol Syst Des Eng 2017;2:616-623. https://doi.org/10.1039/C7ME00063D.

[94]   An CJ, Kang YH, Song H, Jeong Y, Cho SY. High-performance flexible thermoelectric generator by control of electronic structure of directly spun carbon nanotube webs with various molecular dopants. J Mater Chem A, 2017;5:15631-15639. https://doi.org/10.1039/C7TA02509B.

[95]   Chen J, Liu B, Gao X, Xu D. A review of the interfacial characteristics of polymer nanocomposites containing carbon nanotubes. RSC Adv 2018;8:28048-28085. https://doi.org/10.1039/C8RA04205E.

[96]   Rhazi ME, Majid S, Elbasri M, Salih FE, Oularbi L, Lafdi K. Recent progress in nanocomposites based on conducting polymer: application as electrochemical sensors. Int Nano Lett 2018;8(2):79-99. https://doi.org/10.1007/s40089-018-0238-2.

[97]   Vasile C. Polymeric nanocomposites and nanocoatings for food packaging: A review. Mater (Basel) 2018;11(10):1834. https://doi.org/10.3390/ma11101834.

[98]   Müller K, Bugnicourt E, Latorre M, Jorda M, Echegoyen Sanz Y, Lagaron JM, Miesbauer O, Bianchin A, Hankin S, Bölz U, Pérez G, Jesdinszki M, Lindner M, Scheuerer Z, Castelló S, Schmid M. Review on the processing and properties of polymer nanocomposites and nanocoatings and their applications in the packaging, automotive and solar energy fields. Nanomater (Basel) 2017:7(4). https://doi.org/10.3390/nano7040074.

[99]   Khan W, Sharma R, Saini P. Carbon nanotube-based polymer composites: synthesis, properties and applications. In Berber MR, Hafez IH (eds) carbon nanotubes-current progress of their polymer composites. IntechOpen 2016. https://doi.org/10.5772/62497.

[100]   Blattmann CO Pratsinis SE. Single-Step Fabrication of Polymer Nanocomposite Films. Mater (Basel) 2018;11(7):1177. https://doi.org/10.3390/ma11071177.

[101]   Montgomery DS, Hewitt CA, Barbalace R, Jones T, Carroll DL. Spray doping method to create a low-profile high-density carbon nanotube thermoelectric generator. Carbon, 2016;96:778-781. https://doi.org/10.1016/j.carbon.2015.09.029.

[102] Jin H, Li J, Iocozzia J, Zeng X, Wei P, Yang C, Liu Z, He JH, Zhu T, Wang J, Lin Z, Wang S. Hybrid Organic-Inorganic Thermoelectric Materials and Devices. Angew Chem Int Ed 2019. https://doi.org/10.1002/anie.201909082.

[103] Li C, Jiang F, Liu C, Wang W, Li X, Wang T, Xu J. A simple thermoelectric device based on inorganic/organic compositethin film for energy harvesting. Chem Eng J 2017;320:201-210. https://doi.org/10.1016/j.cej.2017.03.023.

[104] Meng Q, Jiangd Q, Cai K, Chen L. Preparation and thermoelectric properties of PEDOT:PSS coated Te nanorod/PEDOT:PSS composite films. Org Electron 2019;64. https://doi.org/10.1016/j.orgel.2018.10.010.

[105] Meng Q, Jiang Q, Cai K, Chen L, Preparation and thermoelectric properties of SWCNT/PEDOT:PSS coated tellurium nanorod composite films. J Alloys Compd 2019;778:163-169. https://doi.org/10.1016/j.jallcom.2018.10.381.

[106] Bae E J, Kang YH, Jang K, Lee C, Cho SY. Solution synthesis of telluride-based nano-barbell structures coated with PEDOT:PSS for spray-printed thermoelectric generators. Nanoscale, 2016;8:10885-10890. https://doi.org/10.1039/C5NR07032E.

[107] Hu X, Zhang K, Wang S, Qiu Y. Thermoelectric Properties of Conducting Polymer Nanowire–Tellurium Nanowire Composites. ACS Appl Energy Mater 2018;1(9):4883-4890. https://doi.org/10.1021/acsaem.8b00909.

[108] Wang Y, Yu C, Sheng M, Song S, Deng Y, Individual adjustment of electrical conductivity and thermopower enabled by multiple interfaces in polyaniline-based ternary hybrid nanomaterials for high thermoelectric performances. Adv Mater Interfaces 2018;5(10):1701168. https://doi.org/10.1002/admi.201701168.

[109] Du Y, Liu X, Xu J, Shen SZ. Flexible Bi-Te-based alloy nanosheet/PEDOT:PSS thermoelectric power generators. Mater Chem Front 2019;3:1328-1334. https://doi.org/10.1039/C9QM00087A.

[110] Ju H, Kim J. Fabrication of conductive polymer/inorganic nanoparticles composite films: PEDOT:PSS with exfoliated tin selenide nanosheets for polymer-based thermoelectric devices. Chem Eng J 2016;297:66-73. https://doi.org/10.1016/j.cej.2016.03.137.

[111] Li X, Liu C, Wang T, Wang W, Wang X, Jiang Q, Jiang F, Xu J. Preparation of 2D MoSe2/PEDOT:PSS composite and its thermoelectric properties. Mater Res Express 2017;4:116410. https://doi.org/10.1088/2053-1591/aa99f9.

[112] Wang X, Meng F, Jiang Q, Zhou W, Jiang F, Wang T, Li X, Li S, Lin Y, Xu J. Simple layer-by-layer assembly method for simultaneously enhanced electrical conductivity and thermopower of PEDOT:PSS/ce-MoS2 Heterostructure films. ACS Appl Energy Mater 2018;1(7):3123-3133. https://doi.org/10.1021/acsaem.8b00315.

[113] Saxena N, Čorić M, Greppmair A, Wernecke J, Pflüger M, Krumrey M, Brandt MS, Herzig EM, Müller-Buschbaum P. Morphology-function relationship of thermoelectric nanocomposite films from PEDOT:PSS with silicon nanoparticles. Adv Electron Mater 2017;3(8):1700181. https://doi.org/10.1002/aelm.201700181.

[114] Zheng Z, Luo J, Li F, Liang G, Fan P. Enhanced thermoelectric performance of P-type Sb2Te3 thin films through organic-inorganic hybridization on flexible substrate. Curr Appl Phys 2019;19(4):470-474. https://doi.org/10.1016/j.cap.2019.01.019.

[115] Li C, Qin X, Li Y, Li D, Zhang J, Guo H, Xin H, Song C. Simultaneous increase in conductivity and phonon scattering in a graphene nanosheets/$(Bi_2Te_3)_{0.2}(Sb_2Te_3)0.8$ thermoelectric nanocomposite. J Alloys Compd 2016;661:389-395. https://doi.org/10.1016/j.jallcom.2015.11.217.

[116] Zhang Y, Jia X, Sun H, Sun B, Liu B, Liu H, Kong L, Ma, H. Enhanced thermoelectric performance of nanostructured CNTs/BiSbTe bulk composite from rapid pressure-quenching induced multi-scale microstructure. J Materiomics 2016;2(4):316-323. https://doi.org/10.1016/j.jmat.2016.08.002.

[117] Goo G, Anoop G, Unithrattil S, Kim WS, Lee HJ, Kim HB, Jung M, Park J, Ko HC, Jo JY. Proton-Irradiation Effects on the Thermoelectric Properties of Flexible Bi_2Te_3/PEDOT:PSS Composite Films. Adv Electron Mater 2019;5(4):1-10. https://doi.org/10.1002/aelm.201800786.

[118] Lei J, Zhang D, Guan W, Ma Z, Cheng Z, Wang C, Wang Y. Enhancement of thermoelectric figure of merit by the insertion of multi-walled carbon nanotubes in α-MgAgSb. Appl. Phys. Lett 2018;113: 083901 .https://doi.org/10.1063/1.5042265.

[119] Nonoguchi Y, Nakano M, Murayama T, Hagino H, Hama S, Miyazaki K, Matsubara R, Nakamura M, Kawai T. Simple salt-coordinated n-type nanocarbon materials stable in air. Adv Funct Mater 2016;26(18), 3021-3028. https://doi.org/10.1002/adfm.201600179.

[120] Zaia EW, Gordon MP, Niemann V, Choi J, Chatterjee R, Hsu C, Yano J, Russ B, Sahu A, Urban JJ. Molecular level insight into enhanced n-type transport in solution-printed hybrid thermoelectrics. Adv Energy Mater 2019;9(13):1803469. https://doi.org/10.1002/aenm.201803469.

[121] Chen Y, He M, Liu B, Bazan GC, Zhou J, Liang Z. Bendable n-type Metallic nanocomposites with large thermoelectric power factor. Adv Mater 2016;29(4):1604752. https://doi.org/10.1002/adma.201604752.

[122] Luoa J, Cerretti G, Krause B, Zhan L, Otto T, Jenschke W, Ullrich M, Tremel W, Voit B, Pötschke P. Polypropylene-based melt mixed composites with singlewalled carbon nanotubes for thermoelectric applications: Switching from p-type to n-type by the addition of polyethylene glycol. Polym 2017;108:513-520. https://doi.org/10.1016/j.polymer.2016.12.019.

[123] Wu G, Zhang Z, Li Y, Gao C, Wang X, Chen G. Exploring High-Performance n type thermoelectric composites using amino-substituted rylene dimides and carbon nanotubes. ACS Nano 2017;11(6):5746-5752. https://doi.org/10.1021/acsnano.7b01279.

[124] Gao C, Liu Y, Gao Y, Zhou Y, Zhou X, Yin X, Pan C, Yang C, Wang H, Chen G, Wang L. High-performance n-type thermoelectric composites of acridones with tethered tertiary amines and carbon nanotubes. J Mater Chem A, 2018;6:20161-20169. https://doi.org/10.1039/C8TA08045C.

[125] Wan C, Tian R, Kondou M, Yang R, Zong P, Koumoto K. Ultrahigh thermoelectric power factor in flexible hybrid inorganic-organic superlattice. Nat Commun 2017;18:1024. https://doi.org/10.1038/s41467-017-01149-4.

[126] Ju H, Kim J. Chemically exfoliated SnSe nanosheets and their SnSe/Poly(3,4ethylenedioxythiophene):Poly(styrenesulfonate) composite films for polymer based thermoelectric applications. ACS NANO 2016;10(6):5730-5739. https://doi.org/10.1021/acsnano.5b07355.

[127] Cao Z, Koukharenko E, Tudor M.J, Torah R.N, Beeby S.P. Flexible screen printed thermoelectric generator with enhanced processes and materials. Sensors and Actuators A: Physical 2016;238:196-206. https://doi.org/10.1016/j.sna.2015.12.016.

[128] Varghese T, Hollar C, Richardson J, Kempf N, Han C, Gamarachchi P, Estrada D, Mehta RJ, Zhang Y.High-performance and flexible thermoelectric films by screen printing solution-processed nanoplate crystals. Scientific Reports 2016;6: 33135. https://doi.org/10.1038/srep33135.

[129] Chen B, Kruse M, Xu B, Tutika R, Zheng W, D. Bartlett M, Wu Y, C. Claussen J. Flexible thermoelectric generators with inkjet-printed bismuth telluride nanowires and liquid metal contacts. Nanoscale 2019;11: 5222-5230.https://doi.org/10.1039/c8nr09101c.

[130] Zhang Z, Qiu J, Wang S. Roll-to-roll printing of flexible thin-film organic thermoelectric devices. Manufacturing Letters 2016;8:6-10.https://doi.org/10.1016/j.mfglet.2016.04.002.

[131] Stepien L, Roch A, Schlaier S, Dani I, Kiriy A, Simon F, V. Lukowicz M, Leyens C. Investigation of the Thermoelectric Power Factorof KOH-Treated PEDOT:PSS Dispersions forPrinting Applications. Energy Harvesting and Systems 2016;3(1):101–111. https://doi.org/10.1515/ehs-2014-0060.

[132] Liu L, Sun Y, Li W, Zhang J, Huang X, Chen Z, Sun Y, Di C, Xu W, Zhu D. Flexible unipolar thermoelectric devices basedon patterned poly[Kx(Ni-ethylenetetrathiolate)]thin films. Materials Chemistry 2017;1:2111-2116. https://doi.org/10.1039/C7QM00223H.

[133] Wu Q, Hu J. A novel design of wearable thermoelectric generator based on 3D fabric structure. Smart Materials and Structures 2017;26(4). https://doi.org/10.1088/1361-665X/aa5694.

[134] Ito M, Koizumi T, Kojima H, Saitob T, Nakamura M. From materials to device design of a thermoelectric fabric for wearable energy harvesters. Journal of Materials Chemistry A 2017;5: 12068-12072. https://doi.org/10.1039/C7TA00304H.

[135] Jung KK, Jung Y, Choi CJ, Lee JM, Ko JS. Flexible thermoelectric generator with polydimethyl siloxane in thermoelectric material and substrate. Current Applied Physics 2016;16:1442-1448. https://doi.org/10.1016/j.cap.2016.08.010.

[136] Bae EJ, Kang YH, Jang KS, Cho SY.Enhancement of Thermoelectric Properties of PEDOT:PSS and Tellurium-PEDOT:PSS Hybrid Composites by Simple Chemical Treatment. Scientific Reports 2016;6: 18805. https://doi.org/10.1038/srep18805.

[137] Bae EJ, Kang YH, Lee C, Cho SY. Engineered Nanocarbon Mixing for Enhancing Thermoelectric Properties of Telluride-PEDOT:PSS Nanocomposite. Journal of Materials Chemistry A 2017;5: 17867-17873. https://doi.org/10.1039/C7TA04280A.